

Hadamard Matrix Guided Online Hashing

Mingbao Lin · Rongrong Ji · Hong Liu · Xiaoshuai Sun · Shen Chen · Qi Tian

Received: date / Accepted: date

Abstract Online image hashing has attracted increasing research attention recently, which receives large-scale data in a streaming manner to update the hash functions on-the-fly. Its key challenge lies in the difficulty of balancing the learning timeliness and model accuracy. To this end, most works follow a supervised setting, *i.e.*, using class labels to boost the hashing performance, which defects in two aspects: First, strong constraints, *e.g.*, orthogonal or similarity preserving, are used, which however are typically relaxed and lead to large accuracy drop. Second, large amounts of training batches are required to learn the up-to-date hash functions, which largely increase the learning complexity. To handle the above challenges, a novel supervised online hashing scheme termed **Hadamard Matrix Guided Online Hashing** (HMOH) is proposed in this paper. Our key innovation lies

in introducing Hadamard matrix, which is an orthogonal binary matrix built via Sylvester method. In particular, to release the need of strong constraints, we regard each column of Hadamard matrix as the target code for each class label, which by nature satisfies several desired properties of hashing codes. To accelerate the online training, LSH is first adopted to align the lengths of target code and to-be-learned binary code. We then treat the learning of hash functions as a set of binary classification problems to fit the assigned target code. Finally, extensive experiments demonstrate the superior accuracy and efficiency of the proposed method over various state-of-the-art methods. Codes are available at <https://github.com/lmbxmu/mycode>.

Keywords Binary Code · Online Hashing · Hadamard Matrix · Image Retrieval

Mingbao Lin¹
lmbxmu@stu.xmu.edu.cn

✉ Rongrong Ji^{1,2}
rrji@xmu.edu.cn

Hong Liu¹
lynnliu.xmu@gmail.com

Xiaoshuai Sun^{1,2}
xiaoshuaisun.hit@gmail.com

Shen Chen¹
chenshen@stu.xmu.edu.cn

Qi Tian³
tian.qi1@huawei.com

¹ Media Analytics and Computing Laboratory, Department of Artificial Intelligence, School of Informatics, Xiamen University, China.

² Peng Cheng Laboratory, Shenzhen, China.

³ Huawei Noah's Ark Lab, China.

1 Introduction

Coming with the ever-increasing amount of visual big data, image hashing has attracted extensive research attention in the past decade (Weiss et al., 2009; Wang et al., 2010; Liu et al., 2012; Gong et al., 2013; Liu et al., 2014; Shen et al., 2015; Gui et al., 2018; Wang et al., 2018; Liu et al., 2018; Yang et al., 2018; Deng et al., 2019a,b). Most existing works are designed to train hash functions one-off from a given collection of training data with/without supervised labels. However, such a setting cannot handle the dynamic scenario where data are fed into the system in a streaming fashion. Therefore, online hashing has been investigated recently (Huang et al., 2013, 2017; Leng et al., 2015; Cakir and Sclaroff, 2015; Cakir et al., 2017a,b; Chen et al., 2017; Lin et al., 2019), which receives streaming data online to update the hash functions instantly. Online hashing merits in its superior efficiency in training and its timeliness in coping with the data variations.

The goal of online hashing is to update hash functions from the upcoming data batch while preserving the discriminability of binary codes for the past streaming data. Existing works in online hashing can be categorized into either supervised methods or unsupervised methods. For supervised methods, representative works include, but not limited to, OKH (Huang et al., 2013, 2017), AdaptHash (Cakir and Sclaroff, 2015), OSH (Cakir et al., 2017a), MIHash (Cakir et al., 2017b) and BSODH (Lin et al., 2019). For unsupervised methods, one can refer to SketchHash (Leng et al., 2015) and FROSH (Chen et al., 2017). In general, supervised online hashing methods typically achieves better results over unsupervised ones, which is mainly due to the use of labels to boost the hashing performance.

So far, online hashing retains as an open problem. Its major challenge lies in the difficulty to make a tradeoff between model accuracy and learning efficiency. To explain more explicitly, there exist two issues: First, existing online hashing methods rely on strong constraints to design robust hash functions, *e.g.*, orthogonality (Cakir and Sclaroff, 2015; Leng et al., 2015; Chen et al., 2017) and similarity preservation (Huang et al., 2013, 2017; Cakir et al., 2017b; Lin et al., 2019), which however need to be relaxed in optimization and therefore lead to large accuracy drop. Second, as validated in Sec. 4.2, existing online hashing methods require large amounts of training data to gain satisfactory results, which inevitably leads to low efficiency. To handle the first issue, the work in (Cakir et al., 2017a) proposed to learn Error Correcting Output Codes (ECOC) to eliminate the heavy constraints in optimization. However, the quality of ECOC remains inferior, which will lead to information loss as the streaming data grows. Besides, the use of online boosting in (Babenko et al., 2009) brings additional training burden. In terms of the second issue, to our best knowledge, there is no work focusing on accelerating the online training, which remains as an open problem.

In this paper, we propose a simple yet effective online hashing method, termed **Hadamard Matrix Guided Online Hashing (HMOH)** to solve the aforementioned problems. Our key innovation lies in the introduction of Hadamard matrix, each column of which serves as the target code to guide the learning of hash functions. First, we propose to generate a Hadamard matrix via the Sylvester method (Sylvester, 1867), which assigns individual column randomly to the streaming data with the same class label as their binary codes. The Hadamard matrix by nature satisfies several desired properties of hashing, *e.g.*, orthogonality and balancedness, which are beneficial to guiding the learning of hash. Second, to align the size of Hadamard matrix with the to-be-learned binary codes, we further employ locality sensitive hashing (LSH) (Gionis et al., 1999) to reduce the length of Hadamard codes, which has been proven to be effective in the following context. Notably,

both Hadamard matrix and LSH can be efficiently applied online, *i.e.*, Hadamard matrix can be generated offline and LSH consisting of random projections is data-independent (Datar et al., 2004). Importantly, no extra training is needed, which differs our method from the existing online hashing (Cakir et al., 2017a) where the ECOC codebook is generated on-the-fly. Third, the assigned binary codes are regarded as virtual category labels (+1 or -1), upon which the hash function is decomposed into a set of binary classification problems that can be well addressed by off-the-shelf online binary classification methods (Freund and Schapire, 1999; Liu et al., 2015; Goh et al., 2001). Last, to preserve the information of the past streaming data while distilling the core knowledge of the current data batch, we further ensemble the learned models in previous rounds, which further boosts the retrieval performance. Extensive experiments on four benchmarks, *i.e.*, CIFAR-10, Places205, MNIST and NUS-WIDE, show that the proposed HCOH achieves better or competitive results to the state-of-the-art methods (Huang et al., 2013; Leng et al., 2015; Cakir and Sclaroff, 2015; Cakir et al., 2017a,b; Lin et al., 2019).

The rest of this paper is organized as follows: In Sec. 2, the related works are discussed. The proposed HMOH and its optimization are presented in Sec. 3. Sec. 4 reports our quantitative evaluations and analysis. Finally, we conclude this paper in Sec. 5.

2 Related Work

There are increasing endeavors of online hashing made in the recent years. In generally, online hashing updates the hash functions sequentially and instantly along with the arriving data batch. According to the different types, existing online hashing can be categorized into either supervised methods or unsupervised methods. The former includes, but not limited to, Online Kernel Hashing (OKH) (Huang et al., 2013, 2017), Adaptive Hashing (AdaptHash) (Cakir and Sclaroff, 2015), Online Supervised Hashing (OSH) (Cakir et al., 2017a), Online Hashing with Mutual Information (MIHash) (Cakir et al., 2017b) and Balanced Similarity for Online Discrete Hashing (BSODH) (Lin et al., 2019). The latter includes, but not limited to, Online Sketching Hashing (SketchHash) (Leng et al., 2015) and Faster Online Sketching Hashing (FROSH) (Chen et al., 2017).

Unsupervised methods consider the inherent properties among data, *e.g.*, distribution and variance, to conduct online hashing. The design of existing unsupervised online hashing is partially inspired from the idea of “data sketching” (Liberty, 2013), where a large dataset is summarized by a much smaller data batch that preserves the properties of interest. For instance, Online Sketching Hashing (Sketch-Hash) was proposed in (Leng et al., 2015), which maximizes the variance of every hashing bit among the sketched data

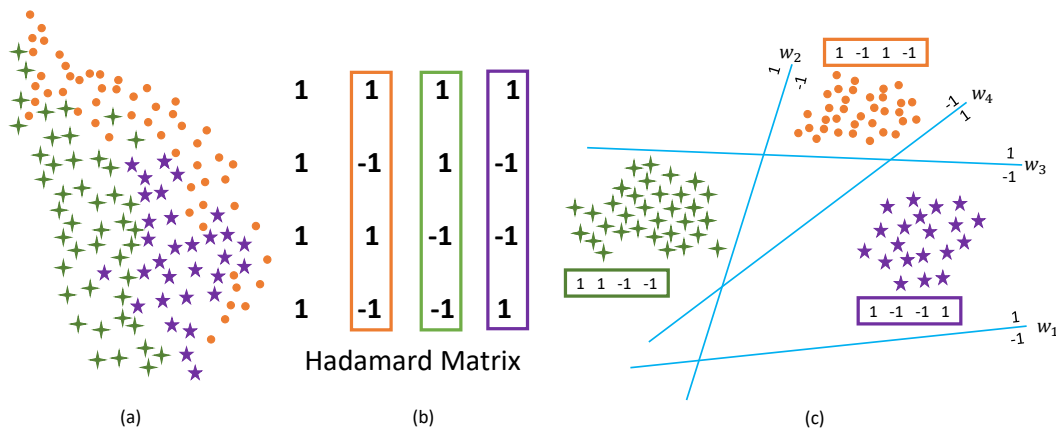


Fig. 1 The proposed Hadamard Matrix Guided Online Hashing framework. Each time when a set of streaming data arrives (a), the data points from the same class (denoted by one common shape and color) are assigned with a column (denoted by the same color) from a pre-generated Hadamard Matrix as the target code ($r^* = 4$ bits in this case) to be learned in the Hamming space (b). And each row is regarded as a set of binary labels (-1 or +1). The goal of our framework is to learn r^* separate binary classifiers to predict each bit (c).

and adopts an efficient variant of SVD decomposition to learn hash functions. A faster version of SketchHash, termed FROSH, was proposed in (Chen et al., 2017) to reduce the training time. FROSH adopts the Subsampled Randomized Hadamard Transform (SRHT) (Lu et al., 2013) to speed up the data sketching process in SketchHash.

Supervised methods take advantage of label information to assist the learning of hash functions. To our best knowledge, Online Kernel Hashing (OKH) (Huang et al., 2013, 2017) is the first of this kind. OKH designs a prediction loss by using pairwise data and is optimized via a passive-aggressive strategy (Crammer et al., 2006), based on which the updated hashing model is able to retain information learned in the previous rounds and adapt to the data in the current round. Similar to OKH, Adaptive Hashing (AdaptHash) (Cakir and Sclaroff, 2015) also assumes that the pairs of points arrive sequentially. A hinge loss (Norouzi and Blei, 2011) is defined to narrow the distance between similar pairs and to enlarge that between dissimilar ones. Then Stochastic Gradient Descent (SGD) is deployed to update the hash functions. In (Cakir et al., 2017a), a two-step hashing framework was introduced, where binary Error Correcting Output Codes (ECOC) (Jiang and Tu, 2009; Kittler et al., 2001; Schapire, 1997; Zhao and Xing, 2013) are first assigned to labeled data, and then hash functions are learned to fit the binary ECOC using Online Boosting (Babenko et al., 2009). Cakir *et al.* developed an Online Hashing with Mutual Information (MIHash) (Cakir et al., 2017b). Given an image, MIHash aims to separate the distributions between its neighbors and non-neighbors of Hamming distances. To capture the separability, Mutual Information (Cover and Thomas, 2012) is adopted as the learning objective and SGD is used to renovate the hash functions. Balanced Similarity for Online Discrete Hashing (BSODH) (Lin et al., 2019) was recently proposed to enable

learning hash model on streaming data, which investigates the correlation between new data and the existing dataset. To deal with the data-imbalance issue (*i.e.*, quantity inequality between similar and dissimilar data) in online learning, BSODH adopts a novel *balanced similarity*, which also enables the use of discrete optimization in online learning for the first time.

In principle, supervised online hashing prevails over unsupervised methods by using the additional label information. However, most existing supervised methods simply resort to learning robust binary codes under strong constraints like orthogonality and similarity preservation. On one hand, a large volume of training data is required to obtain a competitive result, leading to poor efficiency. On the other hand, the optimization process cannot be directly deployed with strong constraints. The relaxation process further leads to low accuracy. To sum up, the effectiveness and efficiency of existing online hashing cannot be simultaneously guaranteed, which is the main focus of this paper to address. Note that our solution has a certain similarity to that of OSH (Cakir et al., 2017a), which, as discussed in Sec. 3.3 and Sec. 4.2, fails in both effectiveness and efficiency.

A preliminary conference version of this work was presented in (Lin et al., 2018). Besides more detailed analysis, this paper differs from our conference version in the following aspects: 1) Instead of simply using linear regression to learn the hash mapping, we further transfer the online retrieval problem into an online binary classification problem, which can be well solved by off-the-shelf algorithms and has achieved better results. 2) We extend the proposed method to multi-label benchmarks by proposing both “majority principle” and “balancedness principle”. 3) We propose to ensemble the learned model in every round together, which is experimentally demonstrated to be more effective than using the updated model alone. 4) More extensive

experiments are conducted to demonstrate the effectiveness and efficiency of the proposed method.

3 The Proposed Method

In this section, we introduce the proposed HMOH method in details. The overall hashing framework is illustrated in Fig. 1. A column from the Hadamard Matrix Fig. 1(b) is assigned to the newly arriving data from the same class as shown in Fig. 1(a). The assigned code plays as the target code in the Hamming space. The goal of the proposed method is to learn a set of binary classifiers to fit the target code as shown in Fig. 1(c).

3.1 Problem Definition

Suppose the dataset is formed by a set of n vectors, $\mathbf{X} = \{\mathbf{x}_i\}_{i=1}^n \in \mathbb{R}^{d \times n}$, and accompanied by a set of class labels $\mathbf{L} = \{l_i\}_{i=1}^n \in \mathbb{N}^n$. The goal of hashing is to learn a set of hashing codes $\mathbf{B} = \{\mathbf{b}_i\}_{i=1}^n \in \{-1, +1\}^{r \times n}$ such that a desired neighborhood structure is preserved. This is achieved by projecting the dataset \mathbf{X} using a set of r hash functions $H(\mathbf{X}) = \{h_i(\mathbf{X})\}_{i=1}^r$, *i.e.*,

$$\mathbf{B} = H(\mathbf{X}) = \text{sign}(\mathbf{W}^T \mathbf{X}), \quad (1)$$

where $\mathbf{W} = \{\mathbf{w}_i\}_{i=1}^r \in \mathbb{R}^{d \times r}$ is the projection matrix and \mathbf{w}_i is the i -th hash function. The sign function $\text{sign}(x)$ returns $+1$ if the input variable $x > 0$, and -1 otherwise. In the online setting, \mathbf{X} comes in a streaming fashion and is not available once for all. Hence, we denote $\mathbf{X}^t = \{\mathbf{x}_i^t\}_{i=1}^{n_t} \in \mathbb{R}^{d \times n_t}$ as the input streaming data at t -stage, denote $\mathbf{B}^t = \{\mathbf{b}_i^t\}_{i=1}^{n_t} \in \{-1, +1\}^{r \times n_t}$ as the learned binary codes for \mathbf{X}^t , and denote $\mathbf{L}^t = \{l_i^t\}_{i=1}^{n_t}$ as the corresponding label set, where n_t is the size of streaming data at t -stage. Correspondingly, the parameter \mathbf{W} updated at t -stage is denoted as \mathbf{W}^t .

3.2 Kernelization

We use kernel trick to take advantages of linear models and meanwhile enable them to capture non-linear data patterns. It has been theoretically and empirically proven to be able to tackle linearly inseparable data (Kulis and Grauman, 2012; Liu et al., 2012; Huang et al., 2013, 2017). We map data in the original space \mathbb{R}^d to a feature space \mathbb{R}^m through a kernel function based on anchor points. Hence, we have a new representation of \mathbf{x}_i that can be formulated by following:

$$z(\mathbf{x}_i) = [\kappa(\mathbf{x}_i, \mathbf{x}_{(1)}), \kappa(\mathbf{x}_i, \mathbf{x}_{(2)}), \dots, \kappa(\mathbf{x}_i, \mathbf{x}_{(m)})]^T, \quad (2)$$

where $\mathbf{x}_{(1)}, \mathbf{x}_{(2)}, \dots, \mathbf{x}_{(m)}$ are m anchors. Without loss of generality, we simplify $z(\mathbf{x}_i^t)$ as \mathbf{z}_i^t and simplify the kernelized representation of \mathbf{X}^t as \mathbf{Z}^t .

To obtain these anchors, we follow the work in (Huang et al., 2013, 2017) to assume that m data points can be available in the initial stage. The learning process will not start until m data points have been collected. Then these m data points are considered as m anchors used in the kernel trick. In terms of the kernel function, we use the Gaussian RBF kernel, *i.e.*, $\kappa(\mathbf{x}, \mathbf{y}) = \exp(-\|\mathbf{x} - \mathbf{y}\|^2 / 2\eta^2)$, where η^2 is known as the *bandwidth* to be tuned in the learning process.

3.3 The Proposed Framework

In this section, we introduce the framework of the proposed online hashing. We first revisit the online hashing formulation based on the Error Correcting Output Codes (ECOC) (Cakir et al., 2017a), which separates the learning process into two steps: (1) When a new label is observed, the new target code, *i.e.*, a codeword from the ECOC codebook, is assigned to it. (2) All data that shares the same labels is proceeded to fit this codeword. To that effect, (Cakir et al., 2017a) adopts the $0-1$ loss, which denotes whether the hash functions fit the assigned codewords. The exponential loss with convexity is further used to replace $0-1$, and then SGD is applied to enable the optimization of hash functions. To further improve the performance, a boosting scheme that considers previous mappings to update each hash function is used to handle the process of error-correlation.

However, there exist some issues in (Cakir et al., 2017a). First, the performance highly depends on the codebook construction, *e.g.*, the distance between the target codes must be large enough to ensure error-correction. However, the codebook quality is degenerated due to the random construction strategy in (Cakir et al., 2017a). Second, the use of exponential loss and boosting further increases the training time, which is a serious concern in online learning. To sum up, the key points for a successful ECOC-based online hashing fall into *a better ECOC codebook, a loss function with less computation cost and an efficient boosting algorithm*.

In terms of a better ECOC codebook, to our best knowledge, the basic idea of ECOC stems from the model of signal transmission in communication (Peterson and Weldon, 1972). Generally, the use of ECOC to guide the hashing learning contains two phases, *i.e.*, “encoding phase” and “decoding phase”. As shown in Fig. 1(b), in the encoding phase, the data points from the same class are assigned with one common column from the ECOC codebook $\mathbf{C} = \{\mathbf{c}_i\}_{i=1}^{r^*} \in \{-1, +1\}^{r^* \times r^*}$. In the decoding phase, the assigned column $\mathbf{c}_{J(\mathbf{x}_i^t)}$ is regarded as the virtual multiple binary categories, where $J(\mathbf{x}_i^t)$ returns the class label of \mathbf{x}_i^t , *i.e.*, l_i^t . Therefore, in the case of $r^* = r$, *i.e.*, the code length is the same with the size of virtual categories (the

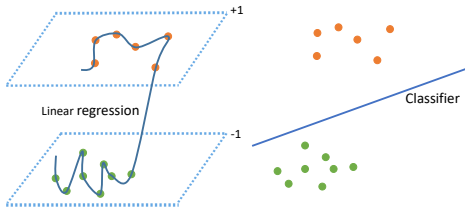


Fig. 2 A comparison between linear regression and classifier. Linear regression tries to fit binary codes with the best hyperplane which goes through the data points. While classifier aims to find a hyperplane to split the data points. Comparing with linear regression, the goal of classifier is much easier.

virtual categories can be seen as the target codes for hashing learning). To this end, the preliminary work, *i.e.*, HCOH (Lin et al., 2018) simply considers the linear regression to fit the virtual categories as follows:

$$\tilde{\phi}(\mathbf{x}_i^t; \mathbf{W}^{t-1}) = \|\mathbf{H}(\mathbf{x}_i^t) - \mathbf{c}_{J(\mathbf{x}_i^t)}\|_F^2, \quad (3)$$

where $\|\cdot\|_F$ is the Frobenius norm of the matrix. Nevertheless, there are some issues in such a learning approach: To enable the optimization of non-convex $\text{sign}(\cdot)$ function in Eq. 1, HCOH has to relax the $\text{sign}(\cdot)$ function ranging in $\{-1, +1\}$, with $\tanh(\cdot)$ function ranging in $(-1, +1)$. On one hand, the relaxation process endures more quantization error. On the other hand, the derivative of $\tanh(\cdot)$ bears more computation burden. Moreover, in the case of low hash bit, it is not appropriate to simply apply the Frobenius norm to fit the target code, due to its inferior performance as shown in (Lin et al., 2018). To analyze the above issues, linear regression attempts to estimate the mapping from the input variables to numerical or continuous output variables. However, the assigned binary codes indeed are in a discrete space (-1 or +1). To fit data with the best hyperplane going through the data points is difficult as illustrated in the left part of Fig. 2. One solution to solve these problems is to use classifier, which attempts to estimate the mapping function from the input variables to discrete or categorical output variables. As shown in the right part of Fig. 2, different with linear regression, the classifier aims to find a hyperplane to split the data points, which is much easier.

On the contrary, in this paper, we consider the hash functions as a set of binary classifiers. And the virtual categories can be used as the corresponding class labels. If $h_k(\mathbf{x}_i) = 1$, a given \mathbf{x}_i belongs to the k -th virtual class, and vice versa. Therefore, the online retrieval problem turns into training r^* separate binary classifiers to predict each bit, which can be well addressed by off-the-shelf methods (Novikoff, 1963; Freund and Schapire, 1999; Liu et al., 2015; Goh et al., 2001). To that effect, we consider the classical Kernelized Perceptron algorithm (Freund and Schapire, 1999). The perceptron based algorithms by nature can be seen as online methods since the binary classifiers are updated in a stream-

ing fashion, which well satisfies the above requirements. By simply removing the $\text{sign}(\cdot)$ in Eq. 1, we obtain the linear functions $\hat{H}(\mathbf{X}^t) = \{\hat{h}_i(\mathbf{X}^t)\}_{i=1}^b$ as:

$$\hat{H}(\mathbf{X}^t) = \mathbf{W}^{t-1T} \mathbf{X}^t, \quad (4)$$

Given a kernelized training data point and its corresponding virtual categories $(\mathbf{z}_i^t, \mathbf{c}_{J(\mathbf{x}_i^t)})$, the loss for perceptron algorithm is as follows:

$$\phi(\mathbf{z}_i^t; \mathbf{W}^{t-1}) = -(\mathbf{c}_{J(\mathbf{x}_i^t)} \odot \mathbf{a}_i^t)^T \hat{H}(\mathbf{z}_i^t), \quad (5)$$

where \odot stands for the Hadamard product (*i.e.*, element-wise product) and \mathbf{a}_i^t is a 0-1 vector with the k -th element \mathbf{a}_{ik}^t defined as 1 if \mathbf{x}_i^t is correctly classified as the virtual label $\mathbf{c}_{J(\mathbf{x}_i^t)k}$ by $\hat{h}_k(\mathbf{x}_i^t)$, and 0 otherwise.

By considering all the data points \mathbf{X}^t at the t -stage, the overall objective function can be re-written as:

$$\begin{aligned} \Phi(\mathbf{Z}^t; \mathbf{W}^{t-1}) &= -\sum_{i=1}^{n_t} (\mathbf{c}_{J(\mathbf{x}_i^t)} \odot \mathbf{a}_i^t)^T \hat{H}(\mathbf{z}_i^t) \\ &= -\text{tr}((\mathbf{c}_{J(\mathbf{X}^t)} \odot \mathbf{A}^t)^T \hat{H}(\mathbf{Z}^t)), \end{aligned} \quad (6)$$

where $\mathbf{A}^t = \{\mathbf{a}_i^t\}_{i=1}^{n_t} \in \mathbb{R}^{r^* \times n^t}$ and $\mathbf{c}_{J(\mathbf{X}^t)} = \{\mathbf{c}_{J(\mathbf{x}_i^t)}\}_{i=1}^{n_t} \in \mathbb{R}^{r^* \times n^t}$.

Above all, the Kernelized Perceptron algorithm merely considers the linear regression without any complex loss to replace the $\text{sign}(\cdot)$, which well satisfies the need for designing a good loss function with less computation cost. Moreover, it also overcomes the inferior performance of the preliminary version (Lin et al., 2018) in low hash bit, as demonstrated later in Sec. 4.2.

3.4 Hadamard Matrix

Above all, the success of online hashing falls in encoding the ECOC matrix \mathbf{C} . To analyze, an efficient hash code should satisfy that the variance of each bit is maximized and the bits are pairwise uncorrelated. That is to say, in Fig. 1(b), half of the data in each row should be +1, and -1 for the other half (Wang et al., 2010). What's more, by designing columns in the ECOC matrix to have maximal Hamming distance from each other, we can get a method that is more resistant to individual bit-flipping errors (misclassification). As above, a robust ECOC codebook \mathbf{C} should satisfy: 1) Maximal Hamming distance between each row, which is for optimal hashing codes. 2) Maximal Hamming distance between each column, which ensures the resistance to misclassification.

To achieve these two goals, we consider the use of Hadamard Matrix (Horadam, 2012) as the backbone to construct the desired ECOC codebook. In particular, on one hand, the Hadamard matrix is an n -order orthogonal matrix, *i.e.*, both its row vectors and column vectors are pairwise

orthogonal, which by nature satisfies the principles of 1) and 2). On the other hand, elements in the Hadamard matrix are either +1 or -1, *i.e.*,

$$\mathbf{H}\mathbf{H}^T = n\mathbf{I}_n, \text{ or } \mathbf{H}^T\mathbf{H} = n\mathbf{I}_n, \quad (7)$$

where \mathbf{I}_n is an n -order identity matrix.

Hence, Hadamard matrix can be used as an efficient ECOC codebook as shown in Fig. 1.

Though the existing theorems that describe the existence of Hadamard matrices of other orders (Paley, 1933; Williamson et al., 1944; Goldberg, 1966; Ockwig et al., 2005), we simply consider the 2^k -order Hadamard matrices in this paper, which can achieve satisfactory performances as shown in Sec. 4. To construct the 2^k -order Hadamard matrices, the entry in the i -th row and the j -th column can be defined as:

$$H_{ij} = (-1)^{(i-1) \times (j-1)}, \quad (8)$$

or it can also be completed by a recursive algorithm as developed in (Sylvester, 1867):

$$H_{2^k} = \begin{bmatrix} H_{2^{k-1}} & H_{2^{k-1}} \\ H_{2^{k-1}} & -H_{2^{k-1}} \end{bmatrix} \text{ and } H_2 = \begin{bmatrix} 1 & 1 \\ 1 & -1 \end{bmatrix}. \quad (9)$$

Since the Hadamard matrix is limited to the 2^k -order in this paper, each data point from the same class label are assigned with one common discriminative column from the Hadamard matrix, and the size of Hadamard matrix r^* can be defined as follows:

$$r^* = \min\{g | g = 2^k, g \geq r, g \geq |\mathbf{L}|, k = 1, 2, 3, \dots\}, \quad (10)$$

where $|\mathbf{L}|$ is the number of class labels in the dataset. Therefore, based on the above discussion, we construct the square Hadamard matrix as $\mathbf{C}_{r^*} \in \{-1, 1\}^{r^* \times r^*}$ as the ECOC codebook. If data with new label is received, we randomly and non-repeatedly select a column representation to construct a virtual label vector for this data. Otherwise, the virtual label previously assigned to instances with the same label is given. Therefore, our scheme does not need to pre-define the category number of the dataset.

3.5 Learning Formulation

The derived formulation is based on the assumption of $r^* = r$ which may not be satisfied¹. To handle this problem, we further use the LSH to transform the virtual labels to obtain the same length of binary codes to the hash functions.

$$\tilde{\mathbf{c}}_{J(x_i)} = \text{sign}(\tilde{\mathbf{W}}^T \mathbf{c}_{J(x_i)}), \quad (11)$$

¹ Take the Places205 dataset as an example: There are in total 205 categories. According to Eq. 10, $r^* = 256$ for the code length r varying from 8 to 128.

where $\tilde{\mathbf{W}} = \{\tilde{\mathbf{w}}_i\}_{i=1}^{r^*} \in \mathbb{R}^{r^* \times r}$ with each $\tilde{\mathbf{w}}_i \in \mathbb{R}^{r^*}$ sampled from the standard Gaussian distribution, *i.e.*, $\tilde{\mathbf{w}}_i \sim N(\mathbf{0}, \mathbf{I})$ and $\mathbf{0}, \mathbf{I}$ are all-zero vector and identity matrix, respectively². In the following, we theoretically demonstrate that $\tilde{\mathbf{c}}_{J(x_i)}$ preserves the main property of $\mathbf{c}_{J(x_i)}$.

Theorem 1: For any vector $\mathbf{w} = [w_1, w_2, \dots, w_{r^*}] \in \mathbb{R}^{r^*}$, each w_i is *i.i.d.* sampled from a Gaussian distribution with zero mean, *i.e.*, $w_i \sim N(0, \sigma^2)$ where σ is the variance. The inner product between \mathbf{w} and \mathbf{c} satisfies

$$P(\mathbf{w}^T \mathbf{c} > 0) = P(\mathbf{w}^T \mathbf{c} < 0). \quad (12)$$

Before the proof of **Theorem 1**, we first briefly give the following Proposition:

Proposition 1: For any $X \sim N(\mu_X, \sigma_X^2)$ and $Y \sim N(\mu_Y, \sigma_Y^2)$, the following satisfies:

$$X + Y \sim N(\mu_X + \mu_Y, \sigma_X^2 + \sigma_Y^2), \quad (13)$$

$$X - Y \sim N(\mu_X - \mu_Y, \sigma_X^2 + \sigma_Y^2), \quad (14)$$

Proof of Theorem 1:

$$\mathbf{w}^T \mathbf{c} = \sum_{i=1}^{r^*} w_i c_i = \sum_{i, c_i=+1} w_i - \sum_{i, c_i=-1} w_i. \quad (15)$$

Based on **Proposition 1** and $w_i \sim N(0, \sigma^2)$, we have

$$\sum_{i, c_i=+1} w_i \sim N(0, \frac{r^*}{2} \sigma^2) \text{ and } (- \sum_{i, c_i=-1} w_i) \sim N(0, \frac{r^*}{2} \sigma^2), \quad (16)$$

And then,

$$(\sum_{i, c_i=+1} w_i - \sum_{i, c_i=-1} w_i) \sim N(0, r^* \sigma^2). \quad (17)$$

The above inference verifies that the inner product between \mathbf{w} and \mathbf{c} obeys the Gaussian distribution with zero mean. Therefore, $P(\mathbf{w}^T \mathbf{c} > 0) = P(\mathbf{w}^T \mathbf{c} < 0)$, which demonstrates the validity of **Theorem 1**.

Further, we denote $P(\text{sign}(\tilde{\mathbf{w}}_j^T \mathbf{c}_{J(x_i)}) = +1)$ as P_{+1} and $P(\text{sign}(\tilde{\mathbf{w}}_j^T \mathbf{c}_{J(x_i)}) = -1)$ as P_{-1} . According to **Theorem 1**, it is easy to derive that $P_{+1} = P_{-1} = 0.5$. In terms of Eq. 11, we denote the number of +1 in the transformed virtual labels $\tilde{\mathbf{c}}_{J(x_i)}$ as M . It is comprehensible that $M \in \{0, 1, \dots, r^*\}$ has a binomial distribution, which is written as:

$$M \sim B(r^*, P_{+1}). \quad (18)$$

The probability function is given by

$$P(M = m) = \binom{r^*}{m} P_{+1}^m P_{-1}^{r^*-m}. \quad (19)$$

² When $r^* = r$, we set $\tilde{\mathbf{W}}$ as an identity matrix and the above equation still holds.

Proposition 2: For any binomial distribution $X \sim B(n, p)$, the probability of $P(X = k)$ reaches the maximal value when $k = k_0$, where

$$k_0 = \begin{cases} (n+1)p & \text{or } (n+1)p - 1, & (n+1)p \in \mathbb{Z}, \\ \lfloor (n+1)p \rfloor, & \text{otherwise,} \end{cases} \quad (20)$$

where $\lfloor \cdot \rfloor$ denotes the integral function. Hence, for Eq. 19, $P(M = m)$ reaches its maximum when $m = \lfloor (r^* + 1)p_{+1} \rfloor = \frac{r^*}{2}$. At this point, the number of -1 in the transformed virtual labels $\tilde{\mathbf{c}}_{J(\mathbf{x}_i^t)}$ is also $\frac{r^*}{2}$.

Therefore, with high probabilities, LSH can balancedly transform each column of the Hadamard matrix, which still gives an effective target code approximate to the requirement of 2). Through similar analysis, we can also obtain that each row of the transformed Hadamard matrix shares similar property, which satisfies the requirement of 1). Hence, applying LSH to transform the virtual categories can well preserve the discrepancy of Hadamard matrix.

Above all, we further reformulate Eq. 6 by LSH-based random hashing as:

$$\begin{aligned} \Phi(\mathbf{Z}^t; \mathbf{W}^{t-1}) &= -\sum_{i=1}^{n_t} (\tilde{\mathbf{c}}_{J(\mathbf{x}_i^t)} \odot \mathbf{a}_i^t)^T \hat{H}(\mathbf{z}_i^t) \\ &= -tr\left((\tilde{\mathbf{c}}_{J(\mathbf{X}^t)} \odot \mathbf{A}^t)^T \hat{H}(\mathbf{Z}^t)\right). \end{aligned} \quad (21)$$

Putting Eq. 4, and Eq. 21 together, we have the following overall objective function:

$$\Phi(\mathbf{Z}^t; \mathbf{W}^{t-1}) = -tr\left((\tilde{\mathbf{c}}_{J(\mathbf{X}^t)} \odot \mathbf{A}^t)^T \mathbf{W}^{t-1T} \mathbf{Z}^t\right). \quad (22)$$

To obtain \mathbf{W}^t , we adopt the classical SGD algorithm as follows:

$$\mathbf{W}^t \leftarrow \mathbf{W}^{t-1} - \lambda \frac{\partial \Phi}{\partial \mathbf{W}^{t-1}}, \quad (23)$$

where λ is the learning rate. And the partial derivative of Φ w.r.t. \mathbf{W}^{t-1} can be derived as:

$$\frac{\partial \Phi}{\partial \mathbf{W}^{t-1}} = -\mathbf{Z}^t (\tilde{\mathbf{c}}_{J(\mathbf{X}^t)} \odot \mathbf{A}^t)^T. \quad (24)$$

3.6 Extended to Multi-label Case

The framework elaborated above assigns one column of the Hadamard Matrix as the target code for data points from the same class, which however, may constrain the application in real-world scenarios since some images may be labeled with multiple classes. To that effect, in this section, we further extend the proposed method to the multi-label case and demonstrate that the generated target code can also effectively approximate to the requirements of 1) and 2) in Sec. 3.4, and thus can preserve the main property of the Hadamard matrix as in Sec. 3.5.

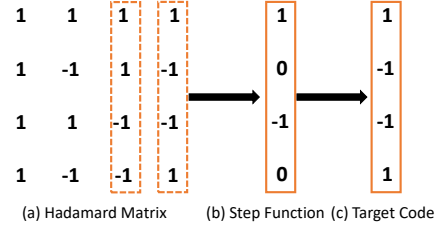


Fig. 3 A toy example of the multi-label case. (a) More than one columns from the Hadamard Matrix will be selected as the target codes for multi-label data. (b) To merge the multiple target codes into one binary vector while preserving the main property of Hadamard matrix, for each bit, we first vote for $+1$ or -1 based on the “majority principle” and vote for 0 if the number of $+1$ and -1 is equal. (c) To balance the number of $+1$ and -1 as much as possible, the 0 elements in (b) will be adjusted to $+1$ or -1 , *i.e.*, “balanced principle”.

In the multi-label case, we first rewrite the label set $\mathbf{L}^t = \{\mathbf{l}_i^t\}_{i=1}^{n_t}$ as $\mathbf{L}^t = \{\mathbf{l}_i^t\}_{i=1}^{n_t}$ where $\mathbf{l}_i^t = \{(l_j^t)\}_{j=1}^{o_t}$ and $(l_j^t)_j$ is the j -th class \mathbf{x}_j^t belongs to and o_t is the total categories of \mathbf{x}_i^t . In this situation, there are o_t target codes extracted from the Hadamard matrix since each class is randomly assigned with one column of the Hadamard matrix. As illustrated in Fig. 3, to fuse these target codes into one vector, we propose to use the “majority principle” and “balancedness principle”. The initial target code for \mathbf{x}_i^t can be defined as:

$$\hat{\mathbf{c}}_{J(\mathbf{x}_i^t)} = step\left(\sum_j^{o_t} \mathbf{c}_{(l_j^t)_j}\right), \quad (25)$$

where $\mathbf{c}_{(l_j^t)_j}$ is the $(l_j^t)_j$ -th column of the Hadamard Matrix. The step function $step(x)$ returns $+1$ if the input variable $x > 0$, 0 if $x = 0$, and -1 , otherwise. For simplicity, we denote the t -th bit of $\hat{\mathbf{c}}_{J(\mathbf{x}_i^t)}$ as \hat{c}_t . The value of \hat{c}_t falls in $\{+1, 0, -1\}$ and is voted based on the “majority principle”. As shown in Fig. 3, $\hat{c}_t = +1$ if the majority elements in the selected t -th row are $+1$; $\hat{c}_t = -1$ if the majority elements in the selected t -th row are -1 ; $\hat{c}_t = 0$ if the numbers of $+1$ and -1 in the t -th row are equal. Finally, the 0 elements in $\hat{\mathbf{c}}_{J(\mathbf{x}_i^t)}$ are further re-assigned with $+1$ or -1 to balance the total number of $+1$ and -1 as far as possible, *i.e.*, “balancedness principle”. After all, we obtain the final target of $\mathbf{c}_{J(\mathbf{x}_i^t)}$.

Below, we analyze that $\mathbf{c}_{J(\mathbf{x}_i^t)}$ in multi-label settings can preserve the main property of the Hadamard codebook. For brevity, we first denote the t -th bit of $\mathbf{c}_{(l_j^t)_j}$ as $(c_j)_t$ and it is easy to obtain:

$$\begin{aligned} \hat{c}_t &= step\left(\sum_j^{o_t} (c_j)_t\right) \\ &= step\left(\sum_j^{o_{t+}} (+1) + \sum_j^{o_{t-}} (-1)\right) \\ &= step(o_{t+} - o_{t-}), \end{aligned} \quad (26)$$

where $o_t = o_{t+} + o_{t-}$, o_{t+} and o_{t-} are the number of $+1$ s and -1 s, respectively.

Theorem 2: At the t -th stage, for any multi-label data point \mathbf{x}_i^t , it satisfies

$$P(o_{t+} > o_{t-}) = P(o_{t+} < o_{t-}). \quad (27)$$

Proof of Theorem 2:

Case 1: o_t is an odd number.

In this situation, it is easy to know that $o_{t+} \neq o_{t-}$. When $o_{t+} \geq \frac{o_t+1}{2}$, $o_{t+} > o_{t-}$, otherwise, $o_{t+} < o_{t-}$. Hence, we have the following equations:

$$P(o_{t+} > o_{t-}) + P(o_{t+} < o_{t-}) = 1. \quad (28)$$

$$P(o_{t+} \geq \frac{o_t+1}{2}) = P(o_{t+} > o_{t-}). \quad (29)$$

$$P(o_{t-} \geq \frac{o_t+1}{2}) = P(o_{t+} < o_{t-}). \quad (30)$$

It's easy to obtain:

$$P(o_{t+} \geq \frac{o_t+1}{2}) = \frac{\sum_{i=\frac{o_t+1}{2}}^{o_t} \binom{\frac{r^*}{2}}{i} \binom{\frac{r^*}{2}}{o_t-i}}{\binom{r^*}{o_t}}. \quad (31)$$

$$P(o_{t-} \geq \frac{o_t+1}{2}) = \frac{\sum_{i=\frac{o_t+1}{2}}^{o_t} \binom{\frac{r^*}{2}}{i} \binom{\frac{r^*}{2}}{o_t-i}}{\binom{r^*}{o_t}}. \quad (32)$$

Combining Eq. 28, Eq. 29, Eq. 30, Eq. 31 and Eq. 32, we obtain:

$$P(o_{t+} > o_{t-}) = P(o_{t+} < o_{t-}) = 0.5. \quad (33)$$

Discussion 1. Based on Eq. 26 and Eq. 33, we have that the t -th bit of $\hat{\mathbf{c}}_{J(\mathbf{x}_i^t)}$, i.e., \hat{c}_t , can be either +1 with 50% probability or -1 with 50% probability.

Case 2: o_t is an even number.

In this situation, the relationships between o_{t+} and o_{t-} are three aspects: 1. When $o_{t+} = \frac{o_t}{2}$, $o_{t+} = o_{t-}$. 2. When $o_{t+} > \frac{o_t}{2}$, $o_{t+} > o_{t-}$. 3. When $o_{t-} > \frac{o_t}{2}$, $o_{t-} > o_{t+}$. Therefore, we have the following equations:

$$P(o_{t+} = o_{t-}) + P(o_{t+} > o_{t-}) + P(o_{t+} < o_{t-}) = 1, \quad (34)$$

$$P(o_{t+} > \frac{o_t}{2}) = P(o_{t+} > o_{t-}), \quad (35)$$

$$P(o_{t-} > \frac{o_t}{2}) = P(o_{t+} < o_{t-}), \quad (36)$$

The probabilities for them are listed as follows:

$$P(o_{t+} = \frac{o_t}{2}) = \frac{\binom{\frac{r^*}{2}}{\frac{o_t}{2}} \binom{\frac{r^*}{2}}{\frac{o_t}{2}}}{\binom{r^*}{o_t}}, \quad (37)$$

$$P(o_{t+} > \frac{o_t}{2}) = \frac{\sum_{i=\frac{o_t}{2}+1}^{o_t} \binom{\frac{r^*}{2}}{i} \binom{\frac{r^*}{2}}{o_t-i}}{\binom{r^*}{o_t}}, \quad (38)$$

$$P(o_{t-} > \frac{o_t}{2}) = \frac{\sum_{i=\frac{o_t}{2}+1}^{o_t} \binom{\frac{r^*}{2}}{i} \binom{\frac{r^*}{2}}{o_t-i}}{\binom{r^*}{o_t}}, \quad (39)$$

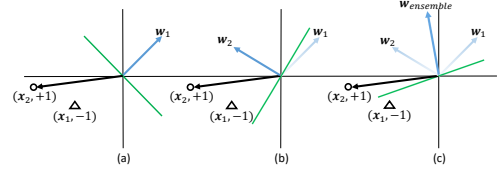


Fig. 4 A toy example of ensembling. (a) \mathbf{w}_1 is learned based on \mathbf{x}_1 , and correctly classifies data point of \mathbf{x}_1 while misclassifying \mathbf{x}_2 . (b) \mathbf{w}_2 is learned based on \mathbf{x}_2 , and correctly classifies data point of \mathbf{x}_2 while misclassifying \mathbf{x}_1 . (c) By taking both \mathbf{w}_1 and \mathbf{w}_2 into considerations, the final $\mathbf{w}_{ensemble}$ correctly classifies both \mathbf{x}_1 and \mathbf{x}_2 .

Combining Eq. 34, Eq. 35, Eq. 36, Eq. 37, Eq. 38 and Eq. 39, we have the following equations:

$$P(o_{t+} = o_{t-}) = \frac{\binom{\frac{r^*}{2}}{\frac{o_t}{2}} \binom{\frac{r^*}{2}}{\frac{o_t}{2}}}{\binom{r^*}{o_t}}. \quad (40)$$

$$P(o_{t+} > o_{t-}) = P(o_{t+} < o_{t-}) = \frac{1 - P(o_{t+} = o_{t-})}{2}. \quad (41)$$

Hence, together with Eq. 33 and Eq. 41, we have the demonstration of **Theorem 2**.

Discussion 2. For Case 2, $P(o_{t+} > o_{t-}) = P(o_{t+} < o_{t-}) < 0.5$. However, when $P(o_{t+} = o_{t-})$, we adopt the “balancedness principle” as demonstrated in Fig. 3 to make sure the balance the number of +1 and -1. Hence, the t -th bit of $\hat{\mathbf{c}}_{J(\mathbf{x}_i^t)}$, i.e., \hat{c}_t , is still either +1 with 50% probability or -1 with 50% probability.

Denote $P(\hat{c}_t = +1)$ as \hat{P}_{+1} and $P(\hat{c}_t = -1)$ as \hat{P}_{-1} . According to *Discussion 1* and *Discussion 2*, we have $\hat{P}_{+1} = \hat{P}_{-1} = 0.5$. We denote the number of +1 in $\mathbf{c}_{J(\mathbf{x}_i^t)}$ as \hat{M} . We can obtain that $\hat{M} \in \{0, 1, \dots, r^*\}$ also has a binomial distribution. According to **Proposition 2**, with a high probability, the proposed “majority principle” and “balancedness principle” can provide an effective target code for the multi-label data, which is approximate to the requirement of 2) in Sec. 3.4. Through similar analysis, it can prove that each bit from different data points sharing at least one different categories satisfies the requirement of 1). Therefore, the proposed “majority principle” and “balancedness principle” can well extend the proposed method to the multi-label dataset.

3.7 Ensemble Learning

When data comes sequentially, the Perceptron algorithm makes at most $(\frac{R}{\gamma})^2$ mistakes (Novikoff, 1963), where the margin γ is defined as $\gamma = \min_{t \in [T]} |\mathbf{x}_t^T \mathbf{w}^*|$ and R is a constant such that $\forall t \in [T], \|\mathbf{x}_t\| \leq R$. It guarantees a tight mistake bound for online classification. But, the case in online retrieval is out of function. Essentially, online classification simply considers prediction on the current streaming data. However, for online retrieval, it has to preserve the information from the past dataset when learning from the

Algorithm 1 Hadamard Matrix Guided Online Hashing

Input: Training data set D with feature space \mathbf{X} and label space \mathbf{L} , the number of hash bits r , the learning rate η , the total number of streaming data batches L .

Output: The hash codes \mathbf{B} for training space \mathbf{X} and the projection coefficient matrix \mathbf{W} .

- 1: Initialize \mathbf{W}^0 and $\mathbf{W}_{ensemble}$ as all-zero matrices.
- 2: Set the value of r^* by Eq. 10.
- 3: Generate Hadamard matrix as stated in Sec. 3.4.
- 4: **if** $r = r^*$ **then**
- 5: Set $\tilde{\mathbf{W}}$ as an identity matrix.
- 6: **else**
- 7: Randomize $\tilde{\mathbf{W}}$ from a standard Gaussian distribution.
- 8: **end if**
- 9: Transform the virtual categories by Eq. 11 or via Sec. 3.6.
- 10: **for** $t = 1 \rightarrow T$ **do**
- 11: Kernelize \mathbf{X}^t by Eq. 2.
- 12: Obtain \mathbf{W}^t by Eq. 23 and Eq. 24.
- 13: $\mathbf{W}_{ensemble} \leftarrow \mathbf{W}_{ensemble} + \mathbf{W}^t$.
- 14: **end for**
- 15: Set $\mathbf{W} = \frac{1}{T} \mathbf{W}_{ensemble}$.
- 16: Compute $\mathbf{B} = \text{sign}(\mathbf{W}^T \mathbf{X})$

current streaming data, since all data points are retrieved in the query stage. Therefore, directly applying Perceptron algorithm to retrieval is far from enough.

To solve it, we consider the ensemble learning to learn a weighted combination of base models from the form of

$$\mathbf{W}_{ensemble} = \sum_{t=1}^T \pi^t \mathbf{W}^t, \quad \text{s.t.} \quad \sum_{t=1}^T \pi^t = 1, \quad (42)$$

where π^t is the tunable parameter. Empirically, we set $\pi^t = \frac{1}{T}$. That is to say, each base model obtains an equal vote on the decision of ensemble model.

Fig. 4 shows a simple example of how ensemble strategy of Eq. 42 works, the quantitative results of which are shown in Sec. 4.5. Generally, the Perceptron algorithm updates each time when a mistake occurs. However, the updated model merely absorbs the misclassified data point to ensure its correctness. As a consequence, the information from the past streaming data loses heavily. Hence, the models updated at different stages are very independent, which is infeasible in a retrieval task. The ensemble strategy to some extent integrates the independent models. Besides, since the weighted parameter π^t is fixed, there has no much time cost to acquire $\mathbf{W}_{ensemble}$ ³.

We summarize the proposed Hadamard Matrix Guided Online Hashing (HMOH) in Alg. 1⁴.

3.8 Time Complexity

From Alg. 1, at each updating stage, the training time is spent on kernelization of \mathbf{X}^t in line 11, the updating of

\mathbf{W}^t in line 12 and the matrix addition for $\mathbf{W}_{ensemble}$ in line 13. In line 11, the time cost is $\mathcal{O}(n_t m d)$. Updating \mathbf{W}^t in line 12 takes $\mathcal{O}(m n_t r^*)$. And it also takes $\mathcal{O}(m r^*)$ in line 13. Above all, the total time complexity for the proposed HMOH is $\mathcal{O}(m n_t d + m n_t r^*)$. What's more, as experimentally demonstrated in Sec. 4.5, the suitable value of n_t is 1 for the proposed method. And we denote $s = \max(d, r^*)$. Hence, without loss of generality, the overall time complexity can be further abbreviated as $\mathcal{O}(m s)$. Hence, our method is scalable.

4 Experiments

In this section, we evaluate our Hadamard matrix guided learning framework for online hashing generation. To verify the performance of the proposed HMOH, we conduct large-scale image retrieval experiments with several state-of-the-art methods (Huang et al., 2013; Leng et al., 2015; Cakir and Sclaroff, 2015; Cakir et al., 2017a,b; Lin et al., 2018, 2019) on four widely-used datasets, *i.e.*, CIFAR-10 (Krizhevsky and Hinton, 2009), Places205 (Zhou et al., 2014a), MNIST (LeCun et al., 1998) and NUS-WIDE (Chua et al., 2009).

4.1 Experimental Settings

Datasets. The *CIFAR-10* contains 60,000 images from 10 classes with each class containing 6,000 instances. Each image is represented by a 4,096-dim feature, which is extracted from the *fc7* layer of the VGG-16 neural network (Simonyan and Zisserman, 2014) pre-trained on ImageNet (Deng et al., 2009). Following the settings in (Cakir et al., 2017b; Lin et al., 2018, 2019), the whole dataset is split into a retrieval set with 59K images and a test set with 1K images. Besides, we randomly sample 20K images from the retrieval set to form a training set to learn the hash functions.

The *Places205* is a subset of the large-scale Places dataset (Zhou et al., 2014a) for scene recognition. It contains 2.5 million images with each image belonging to one of the 205 scene categories. Feature of each image is first extracted from the *fc7* layer of the AlexNet (Krizhevsky et al., 2012) and then represented as a 128-dim feature by performing PCA. To split the entire dataset, following (Lin et al., 2018), we randomly select 20 instances from each category and the remaining is treated as the retrieval set. Lastly, a random subset of 100K images from the retrieval set is used to update the hash functions.

The *MNIST* dataset contains 70K handwritten digit images from 0 to 9. Each image is represented by 784-dim normalized original pixels. According to the experimental settings in (Lin et al., 2019), the dataset is divided into a test set with 100 examples randomly sampled from each class

³ Since it is just a matrix-addition operation at each stage.

⁴ $\tilde{\mathbf{W}}$ is a random matrix that need not be optimized. When $r = r^*$, we set $\tilde{\mathbf{W}}$ as an identity matrix

Table 1 Parameter configurations on the four benchmarks.

Method	CIFAR-10	Places205	MNIST	NUS-WIDE
Kernel	×	√	√	×
σ	×	6	10	×
m	×	800	300	×
λ	0.5	0.01	0.1	0.1
n_t	1	1	1	1

and a retrieval set with all remaining examples. 20K images from the retrieval set is sampled to form a training set.

The *NUS-WIDE* is collected from Flickr, which contains 296,648 images. All images are manually annotated with at least one label from 81 concepts. following (Zhou et al., 2014b; Liu et al., 2018), we preserve 186,577 labeled images from the whole dataset according to the top 10 frequent labels. In this dataset, each image is represented as a 500-dim bag-of-visual-words feature. We choose 2,000 images from this dataset as the query set, and the remaining as the retrieval set. From the retrieval set, 40K images are randomly sampled as the training set.

Evaluation Protocols. We report the experimental results using mean Average Precision (denoted as *mAP*), Precision within a Hamming ball of radius 2 centered on each query (denoted as *Precision@H2*), *mAP vs. different sizes of training instances curves* and their corresponding areas under the *mAP* curves (denoted as *AUC*), Precision of the top K retrieved neighbors (denoted as *Precision@K*) and their corresponding areas under the *Precision@K* curves (denoted as *AUC*), and Precision-Recall Curves.

Notably, when reporting the *mAP* performance on Places205, following the works in (Cakir et al., 2017b; Lin et al., 2018, 2019), we only compute the top 1,000 retrieved items (denoted as *mAP@1,000*) due to its large scale and time consumption. The above metrics are evaluated under hashing bits varying among 8, 16, 32, 48, 64 and 128.

Baseline Methods. We compare our method with representative state-of-the-art online hashing algorithms, including Online Kernel Hashing (OKH) (Huang et al., 2013), Online Sketching Hashing (SketchHash) (Leng et al., 2015), Adaptive Hashing (AdaptHash) (Cakir and Sclaroff, 2015), Online Supervised Hashing (OSH) (Cakir et al., 2017a), Online Hashing with Mutual Information (MIHash) (Cakir et al., 2017b) and Balanced Similarity for Online Discrete Hashing (BSODH) (Lin et al., 2019). Besides, to demonstrate the advantages and improvements of the proposed HMOH, we also compare it with the previous version, *i.e.*, HCOH (Lin et al., 2018). The public MATLAB codes of these methods are available. Our model is also implemented with MATLAB. All the experiments are performed on a server with a 3.60GHz Intel Core I7 4790 CPU and 16G RAM, and the experimental results are averaged over three runs.

Parametric Settings. We describe the parameters to be tuned during the experiments. Since we share the same

dataset configurations on CIFAR-10, Places205 and MNIST, we directly adopt the parameters as described in (Lin et al., 2018, 2019), which have been carefully validated for each method. For NUS-WIDE, we also conduct careful ablation studies for all methods and set the optimal values for all the hyper-parameters. The following describes the parameter configurations for all compared baselines in details.

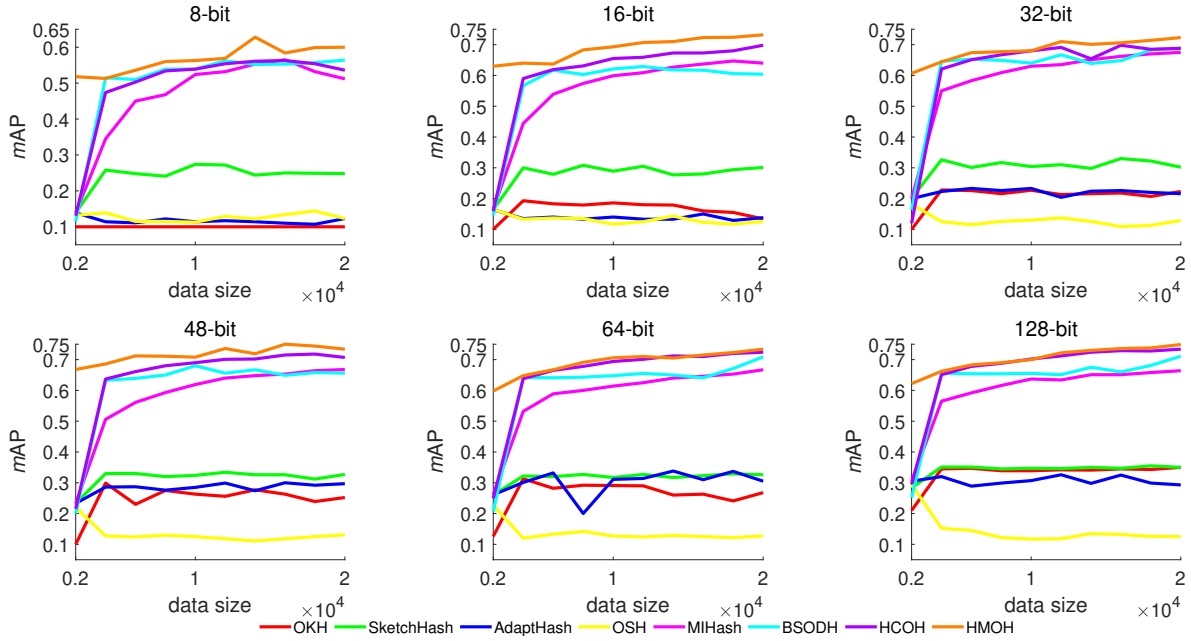
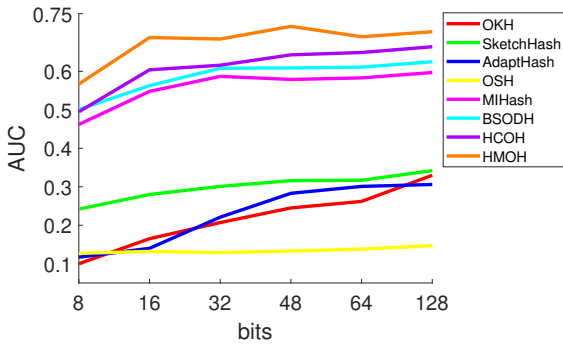
- **OKH:** The tuple (C, α) is set as (0.001, 0.3), (0.0001, 0.7), (0.001,0.3) and (0.001, 0.5) on CIFAR-10, Places205, MNIST and NUS-WIDE, respectively.
- **SketchHash:** The tuple $(sketchsize, batchsize)$ is set as (200, 50), (100, 50), (200, 50) and (200, 50) on CIFAR-10, Places205, MNIST and NUS-WIDE, respectively.
- **AdaptHash:** The tuple (α, λ, η) is set as (0.9, 0.01, 0.1), (0.9,0.01,0.1), (0.8, 0.01, 0.2) and (1, 0.01, 0.5) on CIFAR-10, Places205, MNIST and NUS-WIDE, respectively.
- **OSH:** On all datasets, η is set as 0.1 and the ECOC codebook C is populated the same way as in (Cakir et al., 2017a).
- **MIHash:** The tuple (θ, \mathcal{R}, A) is set as (0, 1000, 10), (0, 5000, 10), (0, 1000, 10) and (0, 2000, 1) on CIFAR-10, Places205, MNIST and NUS-WIDE, respectively.
- **BSODH:** The tuple $(\lambda, \sigma, \eta_s, \eta_d)$ is set as (0.6, 0.5, 1.2, 0.2), (0.3, 0.5, 1.0, 0.0), (0.9, 0.8, 1.2, 0.2) and (0.3, 0.1, 0.4, 1.2) on CIFAR-10, Places205, MNIST and NUS-WIDE, respectively.
- **HCOH:** The tuple (n_t, η) is set as (1, 0.2), (1, 0.1), (1, 0.2) and (1, 0.2) on CIFAR-10, Places205, MNIST and NUS-WIDE, respectively.

Specific descriptions of these parameters for each method can be found in (Huang et al., 2013; Leng et al., 2015; Cakir and Sclaroff, 2015; Cakir et al., 2017a,b; Lin et al., 2019, 2018), respectively. As for the proposed HMOH, we list the parameter configurations on the four benchmarks in Tab. 1. Notably, experiments of the proposed method without kernelization on CIFAR-10 and NUS-WIDE show better results. Hence, kernel trick is not applied in the cases of CIFAR-10 and NUS-WIDE. Detailed analysis is conducted in Sec. 4.5.

Emphatically, for SketchHash (Leng et al., 2015), it has two limitations: First, the training size has to be larger than the code length. Second, the code length has to be smaller than the dimension of input features. Therefore, we show its experimental results with hashing bit being 8, 16, 32, 48 to follow the works in (Lin et al., 2018, 2019) by setting the training size as 50. To evaluate the hashing bit of 64 and 128, the training size is set as 150. In the longer code length (*e.g.*, 256-bit and 512-bit), the experiments can not be conducted on some benchmarks due to the second limitation. All the experiments are run over three times and we report the averaged values in this paper.

Table 2 mAP and Precision@H2 Comparisons on CIFAR-10 with 8, 16, 32, 48, 64 and 128 bits. The best result is labeled with boldface and the second best is with an underline.

Method	mAP						Precision@H2					
	8-bit	16-bit	32-bit	48-bit	64-bit	128-bit	8-bit	16-bit	32-bit	48-bit	64-bit	128-bit
OKH	0.100	0.134	0.223	0.252	0.268	0.350	0.100	0.175	0.100	0.452	0.175	0.372
SketchHash	0.248	0.301	0.302	0.327	0.326	0.351	0.256	0.431	0.385	0.059	0.004	0.001
AdaptHash	0.116	0.138	0.216	0.297	0.305	0.293	0.114	0.254	0.185	0.093	0.166	0.164
OSH	0.123	0.126	0.129	0.131	0.127	0.125	0.120	0.123	0.137	0.117	0.083	0.038
MIHash	0.512	0.640	0.675	0.668	0.667	0.664	0.170	0.673	0.657	0.604	0.500	0.413
BSODH	<u>0.564</u>	0.604	<u>0.689</u>	0.656	0.709	0.711	0.305	0.582	0.691	<u>0.697</u>	0.690	<u>0.602</u>
HCOH	0.536	<u>0.698</u>	0.688	<u>0.707</u>	<u>0.724</u>	<u>0.734</u>	<u>0.333</u>	<u>0.723</u>	<u>0.731</u>	0.694	0.633	0.471
HMOH	0.600	0.732	0.723	0.734	0.737	0.749	0.348	0.756	0.743	0.729	0.710	0.734

**Fig. 5** mAP performance with respect to different sizes of training instances on CIFAR-10.**Fig. 6** AUC curves for mAP on CIFAR-10.

4.2 Results and Discussions

4.2.1 Results on CIFAR-10

The mAP and Precision@H2 values of the proposed HMOH and seven baseline methods on CIFAR-10 dataset are reported in Tab. 2. The mAP vs. different sizes of training instances and their corresponding AUC curves are plotted

in Fig. 5 and Fig. 6, respectively. The Precision@K curves and their corresponding AUC curves are shown in Fig. 7 and Fig. 8, respectively. Finally, Fig. 9 depicts the Precision-Recall curves.

In terms of mAP , from Tab. 2, we can observe that the proposed HMOH obtains the best results in all cases and performs much better than the baselines in some cases, which well demonstrates its effectiveness. Detailedly, compared with the best baseline, *i.e.*, BSODH or MIHash, the proposed HMOH outperforms them by an average percentage of 7.478%. Meanwhile, compared with the previous version of the proposed method, *i.e.*, HCOH, HMOH in our paper obtains an average increase of 4.926%. Regarding the Precision@H2, it can be observed that the proposed method still achieves superior retrieval results by a margin. Quantitatively, compared with BSODH or MIHash, the proposed HMOH achieves satisfactory performance with an average gain of 10.440%. Similarly, HMOH obtains a substantial improvement of 13.971% over the previous version of HCOH. Noticeably, we observe that when the hashing

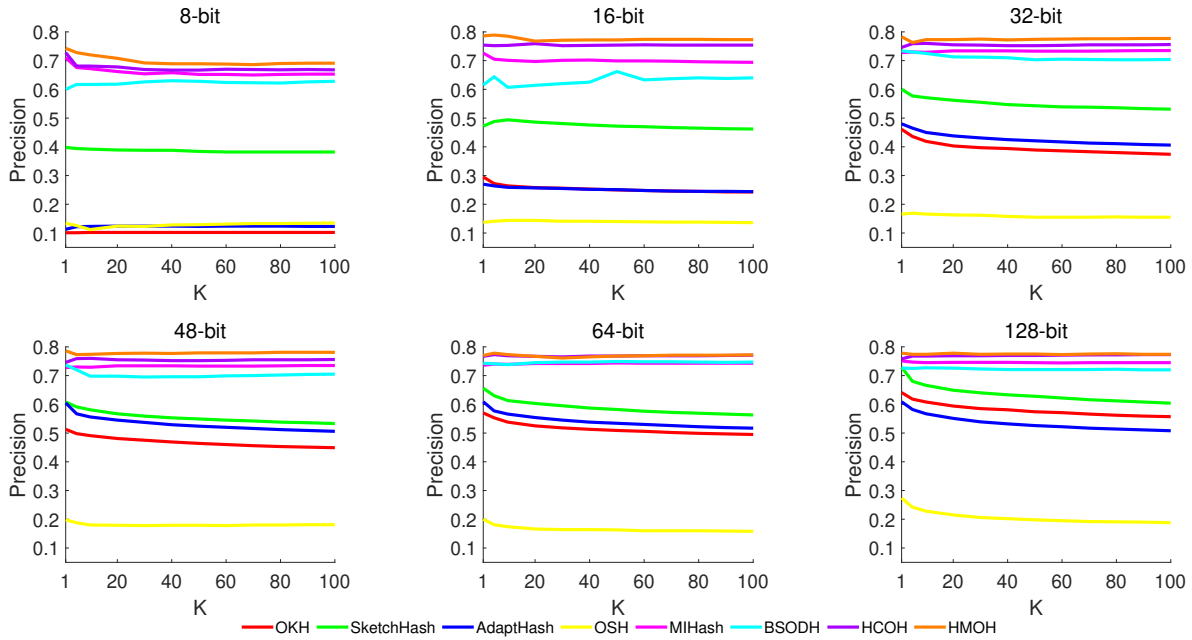


Fig. 7 Precision@K curves of compared algorithms on CIFAR-10.

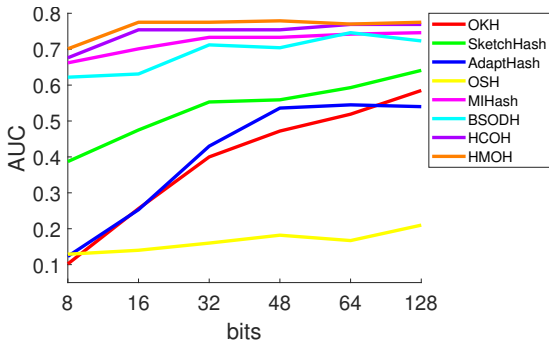


Fig. 8 AUC curves for Precision@K on CIFAR-10.

bit grows up to 128, most of other methods suffer a great deal of performance loss (e.g., MIHash: 0.500 \rightarrow 0.413, BSODH: 0.690 \rightarrow 0.602 and HCOH: 0.633 \rightarrow 0.471). However, the proposed HMOH still shows an increasingly high Precision@H2 result (0.710 \rightarrow 0.734), which demonstrates its robustness.

Next, we further look into the mAP over time for all the online hashing methods as depicted in Fig. 5 and their corresponding AUC results in Fig. 6. Based on Fig. 5, we have the following two observations. First, most cases of all hashing bits, the proposed HMOH yields the best mAP results compared with other methods over time. This can be reflected in their AUC results in Fig. 6. In detail, the proposed HMOH surpasses the best baseline, i.e., BSODH by an average 15.170% gain and outperforms the previous version of HCOH by an average increase of 10.532%. The second observation is that Fig. 5 also implicates a stable generalization ability of the proposed HMOH. That is, HMOH achieves satisfactory performance with only a

small batch of training instances. Especially, taking the case of code length being 48 as an example, when the size of training data is 2K, the proposed HMOH gets an mAP of 0.668 compared with other state-of-the-art baselines, e.g., 0.233 mAP for MIHash, 0.200 mAP for BSODH and 0.215 mAP for HCOH. To achieve similar performance, it takes 20K training instances for MIHash and BSODH, 10K training instances for our previous version of HCOH, which is inefficient.

Moreover, experimental results for Precision@K and their AUC curves are reported in Fig. 7 and Fig. 8, respectively. We can find in Fig. 7 that in low code length (≤ 48), HMOH transcends other methods by a clear margin. While the proposed HMOH shows similar results with its previous version, i.e., HCOH, in large code length (≥ 64), it still holds the first position for all hashing bits. Quantitatively speaking, as far as their AUC performance in Fig. 8, the proposed HMOH consistently outperforms the best baseline by an average of 6.019% AUC gain. And compared with HCOH, our proposed HMOH still outperforms by an average increase of 2.249%. Hence, the proposed HMOH shows a great improvement over the previous version and its effectiveness over other methods.

For further analysis, we plot the Precision-Recall curves in Fig. 9. From Fig. 9, we can observe similar results to those in Tab. 2 (mAP), Fig. 5 and Fig. 7. In most cases, the proposed HMOH and its previous version HCOH consistently outperform all other methods. In the case of 8-bit, BSODH ranks the second. No matter what, the proposed HMOH generally performs the best from short code length to long code length.

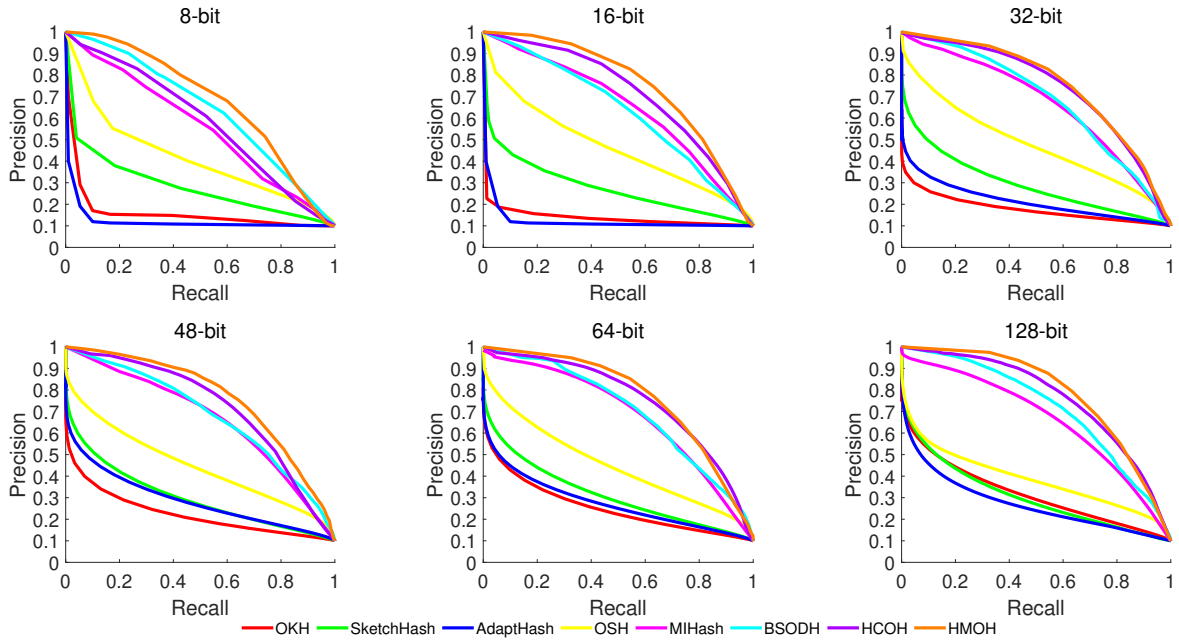


Fig. 9 Precision-Recall curves of compared algorithms on CIFAR-10.

Table 3 $mAP@1,000$ and Precision@H2 Comparisons on Places205 with 8, 16, 32, 48, 64 and 128 bits. The best result is labeled with boldface and the second best is with an underline.

Method	$mAP@1,000$						Precision@H2					
	8-bit	16-bit	32-bit	48-bit	64-bit	128-bit	8-bit	16-bit	32-bit	48-bit	64-bit	128-bit
OKH	0.018	0.033	0.122	0.048	0.114	0.258	0.007	0.010	0.026	0.017	0.217	0.075
SketchHash	0.052	0.120	0.202	0.242	0.274	0.314	<u>0.017</u>	0.066	0.220	0.176	0.274	0.016
AdaptHash	0.028	0.097	0.195	0.223	0.222	0.229	0.009	0.051	0.012	0.185	0.021	0.022
OSH	0.018	0.021	0.022	0.032	0.043	0.164	0.007	0.009	0.012	0.023	0.030	0.059
MIHash	<u>0.094</u>	<u>0.191</u>	0.244	0.288	0.308	0.332	0.022	0.112	0.204	0.242	0.202	0.069
BSODH	0.035	0.174	0.250	0.273	0.308	0.337	0.009	0.101	0.241	<u>0.246</u>	<u>0.212</u>	<u>0.101</u>
HCOH	0.049	0.173	<u>0.259</u>	0.280	<u>0.321</u>	<u>0.347</u>	0.012	0.082	<u>0.252</u>	0.179	0.114	0.036
HMOH	0.102	0.232	0.305	0.314	0.335	0.349	0.014	0.137	0.296	0.262	0.223	0.137

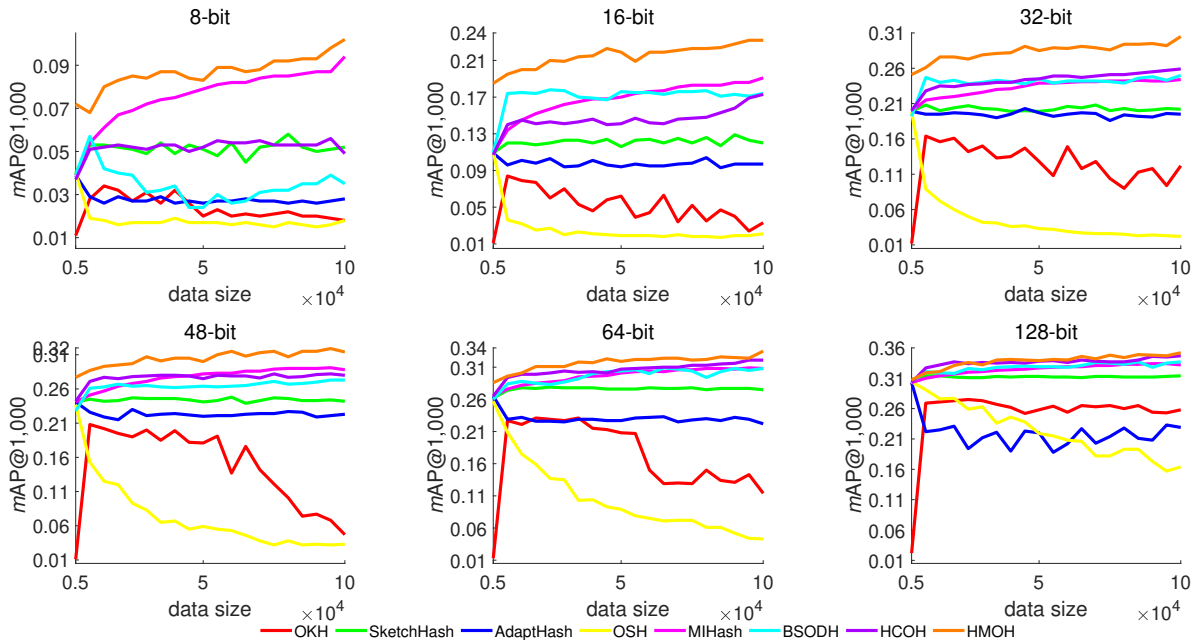


Fig. 10 mAP performance with respect to different sizes of training instances on Places205.

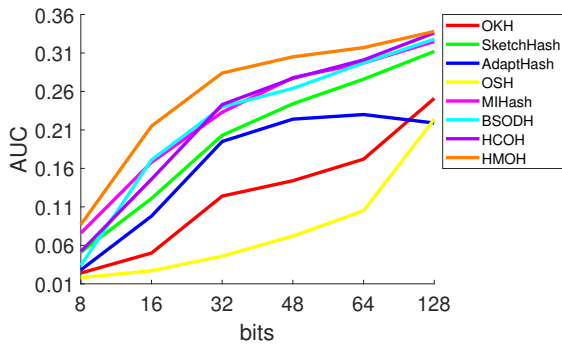


Fig. 11 AUC curves for mAP on Places205.

4.2.2 Results on Places205

Tab. 3 displays the $mAP@1,000$ and Precision@H2 results. Also, Fig. 10 illustrates the $mAP@1,000$ vs. different sizes of training instances comparisons and their AUC results are plotted in Fig. 11. We show the Precision@K curves and their AUC curves in Fig. 12 and Fig. 13, respectively. Besides, the Precision-Recall performance can be found in Fig. 14.

We start with an analysis of the $mAP@1,000$ performance. From Tab. 3, two observations can be derived. First, the proposed HMOH keeps substantially best mAP performance. In particular, HMOH consistently outperforms the best baselines, *i.e.*, MIHash or HCOH, by an average of 13.090%, and transcends our previous version of HCOH by an average increase of 29.662%, respectively. The second observation comes that the proposed HMOH overcomes the drawback of the previous HCOH, *i.e.*, suffering poor performance in low code length (*e.g.*, 8 or 16). As mentioned in (Lin et al., 2018), HCOH is only suitable for learning models with high-dimensional features in low hash bit (4096-D for CIFAR-10, 128-D for Places205 and 784-D for MNIST). Particularly, when the hashing bits are 8 and 16, the proposed HMOH not only ranks first but also obtains an increase of 108.163% and 34.104% compared with the previous HCOH, respectively. Therefore, HMOH can well address the obstacles HCOH suffers, which further demonstrates the effectiveness of the proposed HMOH.

When it comes to the results of Precision@H2 in Tab. 3, we can observe that with hashing bit being 8, the proposed HMOH ranks second and MIHash holds the first position. However, as the code length increases, the proposed HMOH still consistently shows the best. Concretely speaking, in low bit of 8, compared with HMOH, MIHash acquires 57.143% gains. When the code length is more than 8, compared with the state-of-the-art method, *i.e.*, MIHash or BSODH, HMOH shows a relative increase of 18.496% which verifies the superiority of the proposed HMOH. Notably, when the hashing bit is 128, like other methods (MIHash: 0.202 \rightarrow 0.069, BSODH: 0.212 \rightarrow 0.101, HCOH: 0.114 \rightarrow 0.036), the proposed HMOH also drops (0.223 \rightarrow 0.137), which

contradicts with the observation on CIFAR-10. We argue that this is owing to the large scale of Places205 which is in millions. Searching for similar items within a Hamming ball of radius 2 in large code length on a large dataset is tough. Nevertheless, the proposed HMOH drops least and shows best results.

Further, we analyze the results of mAP over time and the corresponding AUC curves in Fig. 10 and Fig. 11, respectively. Generally, the two key observations on CIFAR-10 can also be found in Places205, *i.e.*, superior mAP results over time and good generalization ability. For the superior mAP results over time, we analyze the AUC curves in Fig. 11. To be specific, the proposed HMOH surpasses the best baselines, *i.e.*, MIHash or BSODH by an averaged improvement of 13.006%. And comparing HMOH with its previous version, HCOH (Lin et al., 2018), the proposed HMOH gets an average boost of 24.577%. It can be concluded that, in low hash bit, the proposed HMOH improves quite a lot compared to HCOH. As for the generalization ability, we can find that in most hash bits (except 128), HMOH still obtains relatively high results with only a small number of training data. To take the hash bit of 48 as an example, when the size of training data is 5K, the proposed HMOH gets an mAP of 0.277. However, the state-of-the-art methods suffer lower performance. For example, it is 0.241 mAP for MIHash, 0.228 mAP for BSODH and 0.242 mAP for HCOH. To achieve similar performance, it takes 40K training instances for MIHash, 100K training instances for BSODH, and 80K training instances for our previous version of HCOH. It can be concluded that the proposed HMOH holds good generalization ability.

The Precision@K curves are presented in Fig. 12 and we plot their AUC results in Fig. 13. Though in the case of 128-bit, MIHash and HCOH perform best, the proposed HMOH outranks other methods in other hashing bits. When the hashing bit is 128, MIHash achieves an AUC improvement of 2.579% and HCOH obtains a 1.719% improvement over the proposed HMOH. On the contrary, in other cases, HMOH surpasses MIHash by an average of 6.775% improvements, respectively. Meanwhile, it increases the previous version of HCOH by an average of 29.355%. Especially, it is clear that the proposed HMOH boosts its previous version, *i.e.*, HCOH, by a large margin in low hashing bits.

Fig. 14 shows the Precision-Recall curves on Places205. Generally, the proposed HMOH outperforms all baselines in all cases, which well demonstrates its effectiveness. One common observation for all methods in Fig. 14 is that the areas covered by the Precision-Recall curves all relatively lower when compared with these in Fig. 9. To analyze, the Places205 is a large-scale benchmark, on which it is quite challenging to obtain a high performance. In 8-bit, the improvements for HMOH are not significant because 8

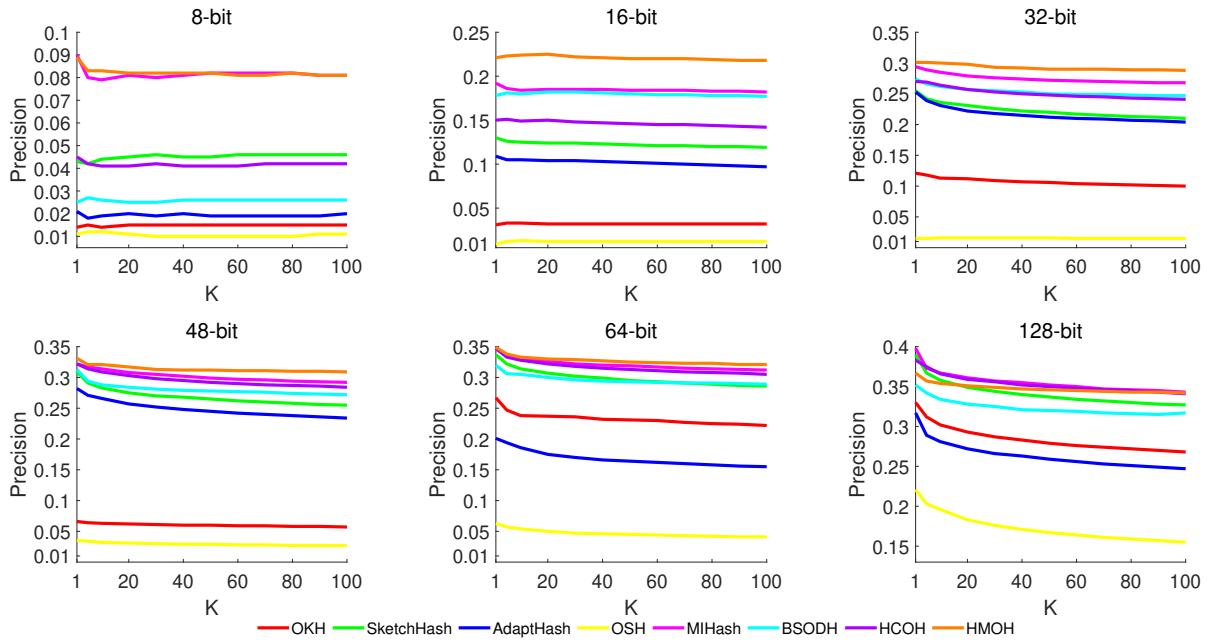


Fig. 12 Precision@K curves of compared algorithms on Places205.

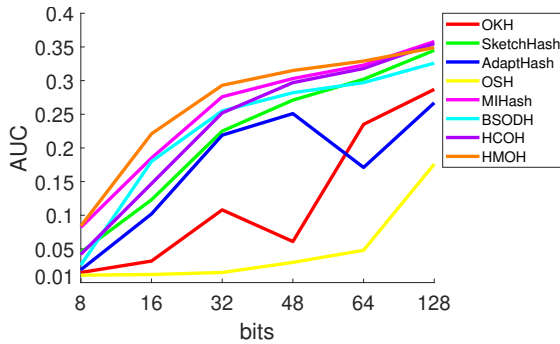


Fig. 13 AUC curves for Precision@K on Places205.

bits can not encode well the abundant information contained in the large-scale Places205. Nevertheless, with the code length increasing, the proposed HMOH still shows a clear better performance.

4.2.3 Results on MNIST

Besides the quantitative evaluation on the above two datasets, we also apply our techniques on MNIST with features of pixel level. The concrete values of mAP and Precision@H2 are filled in Tab. 4. Fig. 15 illustrates the mAP curves under different training instances, and Fig. 16 depicts their AUC performance. The results for Precision@K and their AUC curves can be observed in Fig. 17 and Fig. 18, respectively. Finally, Fig. 19 demonstrates the Precision-Recall curves.

With regards to mAP in Tab. 4, we have the following findings: First, the proposed HMOH is competitive and far better than other methods. More specifically, the state-of-the-art online hashing method, MIHash or BSODH, is

surpassed by the proposed HMOH by large gaps, *i.e.*, an average improvement of 10.401%. Also, the previous version of HCOH is transcended by HMOH by 15.595%. As the second finding, there is a great improvement of the proposed HMOH in low hashing bits (*e.g.*, 8 or 16), which can also be found in Places205 as aforementioned. With code length being 8 and 16, the previous version of HCOH falls behind MIHash and BSODH, which shows its inferiority in low hashing bits. However, the proposed HCOH not only ranks first but also outranks HMOH by an improvement of 38.619% in 8-bit and 17.232% in 16-bit.

With regards to Precision@H2 in Tab. 4, we analyze as follows: First, similar to the performance on Places205, the proposed method ranks second, which is slightly worse than MIHash in the case of 8-bit. And as the code length increases, HMOH keeps substantially best performance. Concretely, when the code length is 8, MIHash gets an improvement of 3.397%. Under other circumstances, compared with MIHash or BSODH, the performance of HMOH increases by an average of 8.924%. What's more, when compared with the previous version, *i.e.*, HCOH, the proposed HMOH obtains a continually averaged growth of 32.330%. Second, we observe that the robustness of the proposed method can be also found on MNIST, which is similar to that on CIFAR-10. As the code length increases to 128-bit, other state-of-the-art methods degrade a lot (MIHash: 0.720 \rightarrow 0.471, BSODH: 0.814 \rightarrow 0.643, HCOH: 0.643 \rightarrow 0.370).

We then evaluate the mAP vs. different sizes of training instances in Fig. 15. Obviously, the curve for the proposed HMOH is above other methods by a largin margin in all hashing bits. To quantitatively evaluate the performance, we

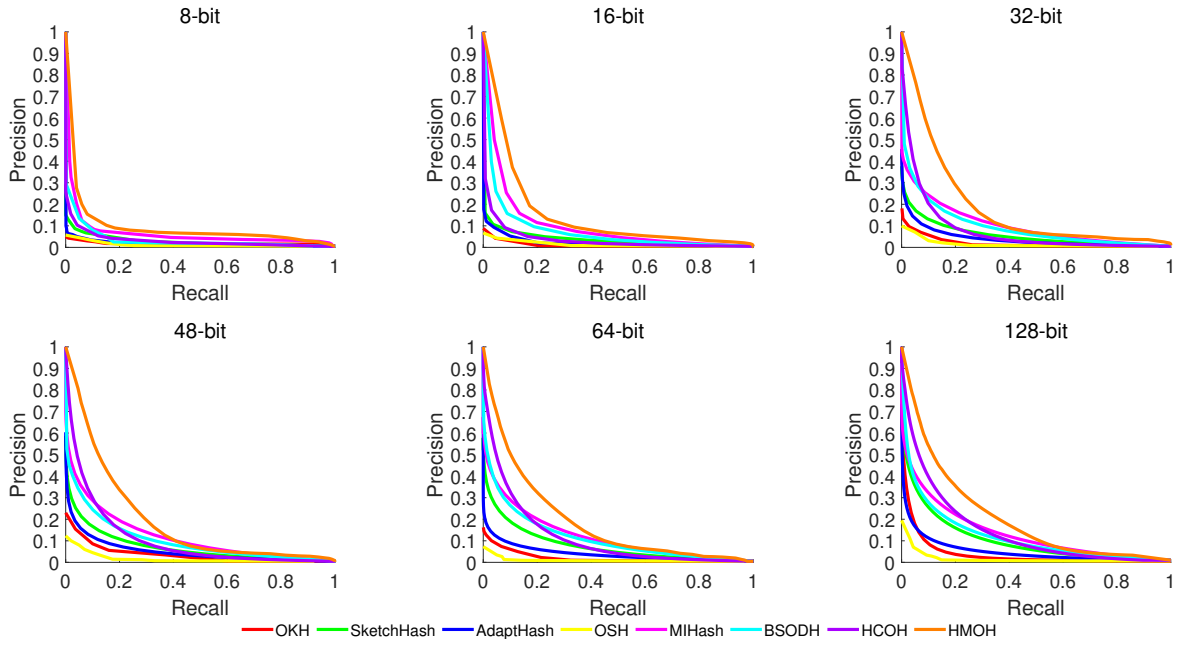


Fig. 14 Precision-Recall curves of compared algorithms on Places205.

Table 4 mAP and Precision@H2 Comparisons on MNIST with 8, 16, 32, 48, 64 and 128 bits. The best result is labeled with boldface and the second best is with an underline.

Method	mAP						Precision@H2					
	8-bit	16-bit	32-bit	48-bit	64-bit	128-bit	8-bit	16-bit	32-bit	48-bit	64-bit	128-bit
OKH	0.100	0.155	0.224	0.273	0.301	0.404	0.100	0.220	0.457	0.724	0.522	0.124
SketchHash	0.257	0.312	0.348	0.369	0.376	0.399	0.261	0.596	0.691	0.251	0.091	0.004
AdaptHash	0.138	0.207	0.319	0.318	0.292	0.208	0.153	0.442	0.535	0.335	0.163	0.168
OSH	0.130	0.144	0.130	0.148	0.146	0.143	0.131	0.146	0.192	0.134	0.109	0.019
MIHash	<u>0.664</u>	<u>0.741</u>	0.744	<u>0.780</u>	0.713	0.681	0.487	0.803	0.814	0.739	0.720	0.471
BSODH	0.593	0.700	0.747	0.743	<u>0.766</u>	0.760	0.308	0.709	<u>0.826</u>	<u>0.804</u>	<u>0.814</u>	<u>0.643</u>
HCOH	0.536	0.708	<u>0.756</u>	0.772	0.759	<u>0.771</u>	0.350	0.800	<u>0.826</u>	0.766	0.643	0.370
HMOH	0.743	0.830	0.847	0.845	0.828	0.826	<u>0.471</u>	0.838	0.869	0.854	0.855	0.857

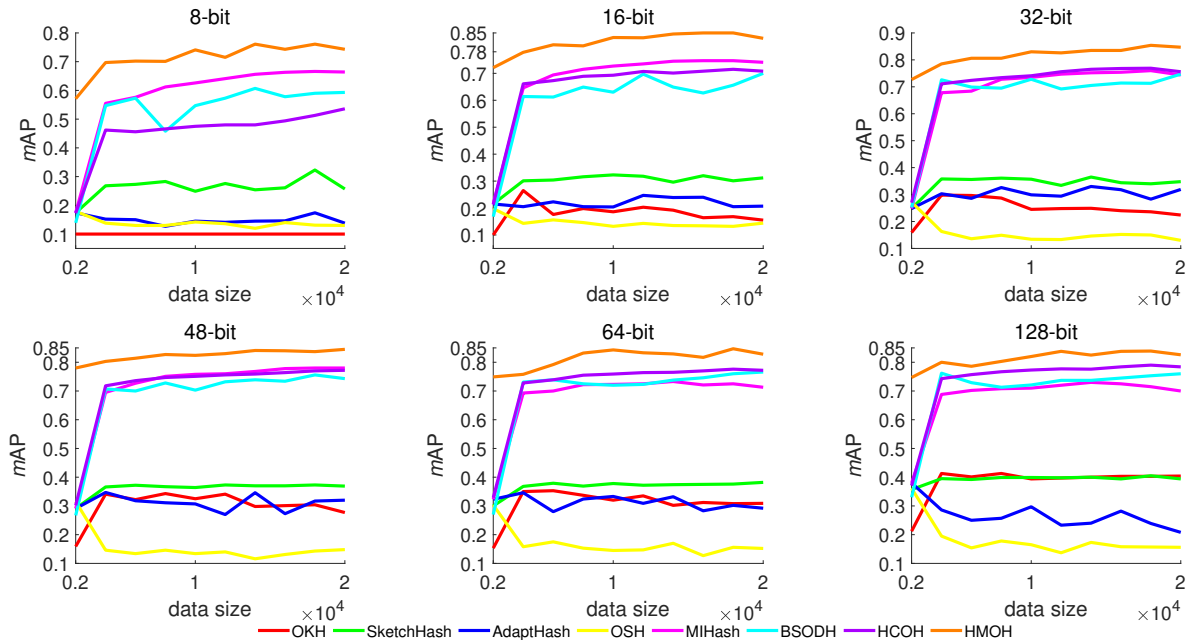


Fig. 15 mAP performance with respect to different sizes of training instances on MNIST.

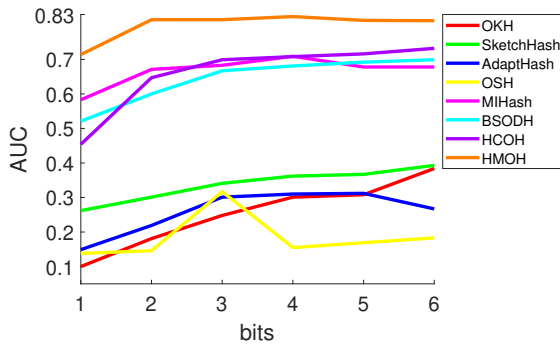


Fig. 16 AUC curves for mAP on MNIST.

move to their corresponding AUC values in Fig. 16, which clearly shows the high performance of the proposed HMOH. Detailedly, compared with the best results between MIHash and BSODH, the proposed HMOH increases by 18.855%. And it is 23.448% compared with its previous version, *i.e.*, HCOH. It’s clear that HMOH improves quite a lot especially in low hashing bits (*e.g.*, 57.269% in 8-bit and 25.966% in 16-bit). Besides, we can derive the generalization ability of the proposed HMOH as well from Fig. 15. That is, HMOH can achieve satisfactory performance with a much smaller batch of training instances. To illustrate, we take the case with 48-bit as an example. When the number of instances is just 2K, HMOH achieves a relatively high result of 0.780, while it is only 0.291 for MIHash, 0.267 for BSODH and 0.302 for HCOH. As the number of training instances increases to 20K, it is 0.780 for MIHash, 0.743 for BSODH and 0.772 for HCOH, while HMOH achieves 0.845. Visibly, HMOH with only 2K training instances already shows competitive performance when compared with MIHash, BSODH and HCOH with training instances as many as 20K.

We plot the Precision@K curves in Fig. 17 and the corresponding AUC results in Fig. 18. Clearly, except the case of 128-bit where our method ranks second, the proposed HMOH shows generally best performance. To be concrete, in terms of the AUC curves for Precision@K, with hashing bit being 128, MIHash gets a result of 0.899 while it is 0.887 for the proposed HMOH. When hashing bit varies from 8 to 64, the proposed HMOH outperforms the best baseline, *i.e.*, MIHash, 1.606% on average. While compared with the previous version of HCOH, it outperforms in all aspects by an average of 5.393%. Again, the proposed HMOH boosts its previous version of HCOH by a large margin especially in low hashing bits.

Lastly, we plot the Precision-Recall curves on MNIST in Fig. 19. Similar to the *mAP* results, the Precision-Recall curve for the proposed HMOH shows significant improvements in all code lengths. Besides, it can be observed that, as the bit increases, the advantage of the proposed HMOH over the state-of-the-art methods decreases. To analyze, on one hand, larger bits can encode more information in the dataset. On the other hand, different with Places205, MNIST

is a simple benchmark. Hence, compared with Fig. 14, the curve areas for most methods are larger. Nevertheless, the proposed HMOH still yields a clearly better result.

4.2.4 Results on NUS-WIDE

For NUS-WIDE, Tab. 5 shows the *mAP* and Precision@H2 results. The *mAP* vs. different sizes of training instances curves and their AUC results are displayed in Fig. 20 and Fig. 21, respectively. Fig. 22 plots the Precision@K curves and their AUC curves are illustrated in Fig. 23. Lastly, the Precision-Recall results are shown in Fig. 24.

We first analyze the *mAP* performance in Tab. 20. As can be observed, the proposed HMOH yields best results in all code lengths. Different with the observations in Tab. 2 (CIFAR-10), Tab. 3 (Places205) and Tab. 4 (MNIST), the BSODH obtains the second best in all bits, outperforming MIHash and HCOH while the performance of MIHash is not so good as on the other three benchmarks. To explain: BSODH adopts the inner-product scheme where the inner product of two hashing codes aims to approximate their similarity matrix ($\{-1, +1\}$). However, the “data-imbalance” issue in online learning disables the learning of BSODH. On NUS-WIDE, the “data-imbalance” issue can be relieved because any two data points are defined as similar if they share at least one same label and the quantitative difference between the number of similar pairs and dissimilar pairs is minor. As for MIHash, given a query, it aims to separate the Hamming distance distributions between its neighbors and non-neighbors. However, the low-level features (bag-of-visual-words) used on NUS-WIDE make it hard to learn the separable distance distributions in Hamming space. Another observation is that the advantage of the proposed HMOH over BSODH is incremental gradually as code length increases (0.001 \rightarrow 0.003 \rightarrow 0.006 \rightarrow 0.010 \rightarrow 0.013 \rightarrow 0.014). On one side, more bits can encode more information contained in the dataset. On the other side, it well demonstrates the efficacy of the proposed “majority principle” and “balancedness principle” on multi-label benchmarks in Sec. 3.6.

Then, we analyze the Precision@H2 in Tab. 5. The performance of the proposed HMOH is similar to that on Places205 and MNIST. In the case of 8-bit, the proposed HMOH ranks second, slightly worse than BSODH and holds the first place in all other cases. Quantitatively, in 8-bit, BSODH obtains 0.719% improvements over the proposed method. As the code length increases, the proposed method surpass the second best method by an improvement of 3.084%, 2.306%, 2.418%, 3.720% and 1.961%, respectively. One observation is that in 128-bit, the proposed HMOH shows a significant performance drop (0.474 \rightarrow 0.468). Nevertheless, the proposed HMOH still gains the best performance compared with the second best BSODH

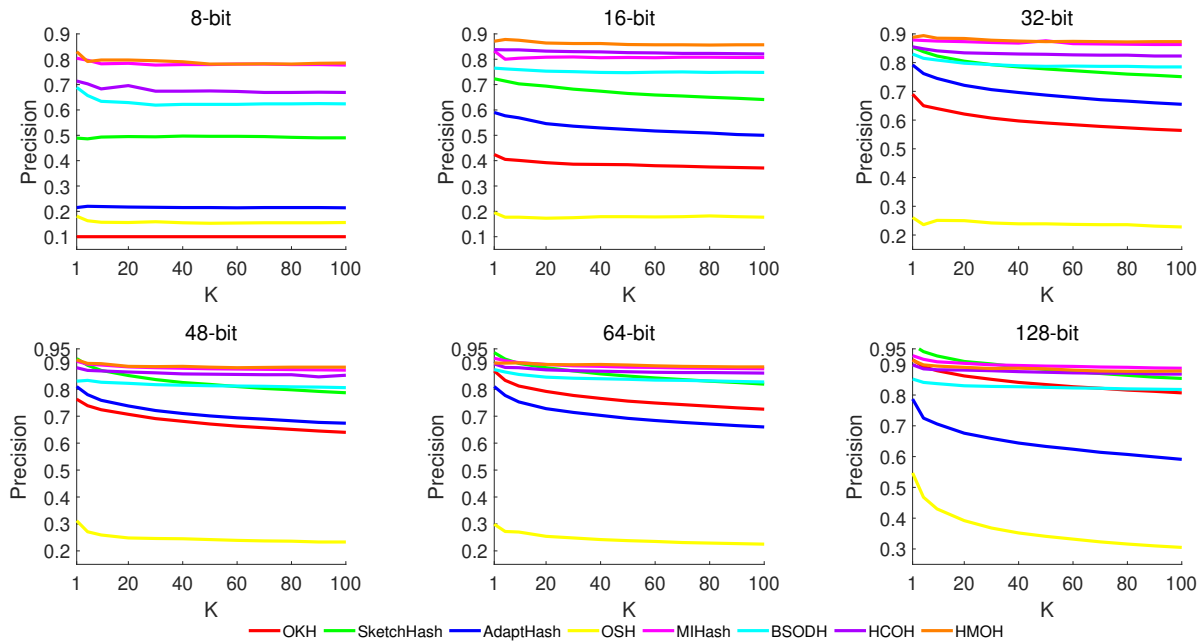


Fig. 17 Precision@K curves of compared algorithms on MNIST.

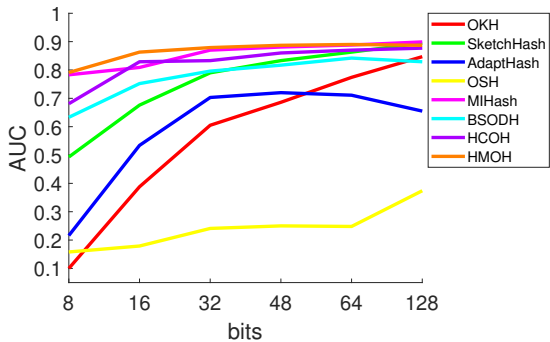


Fig. 18 AUC curves for Precision@K on MNIST.

with only 0.459 Precision@H2 performance. Hence, the superiority of the proposed HMOH on multi-label case is still undoubted.

In Fig. 20, we give a detailed analysis on performance of the mAP vs. different sizes of training instances. Three observations can be obtained as follows: First, the proposed HMOH consistently outperforms others and the second best is BSODH or HCOH. To quantitatively analyze, we turn to the AUC curves in Fig. 21. The proposed HMOH obtains 3.511% (8-bit), 1.602% (16-bit), 3.956% (32-bit), 4.429% (48-bit), 3.480% (64-bit) and 3.944% (128-bit) improvements over the second best. Second, in 8-bit, 16-bit and 32-bit, the proposed method shows a degenerated trend as the training data grows while in 48-bit, 64-bit and 128-bit, the performance increases on the contrary. As an analysis, NUS-WIDE is a relatively large benchmark and it is not enough to encode abundant information as the training data increases in low hashing bits. Nevertheless, the proposed HMOH still shows best efficacy. Third, the proposed HMOH

can obtain fast adaptivity with less training instances. As above, we take 48-bit as an example. When the number of training instance is $4K$, the proposed HMOH achieves mAP of 0.439. While it is 0.417 for the previous version, HCOH, and only 0.359 for BSODH. When the size of training data arrives at $40K$, HCOH obtains mAP of 0.431 while BSODH gains 0.438, both of which still fall behind the performance of the proposed HMOH in $4K$. Hence, the proposed HMOH can be well applied to the multi-label dataset in online learning.

Fig. 22 plots the Precision@K results of all compared methods and Fig. 23 presents the AUC curves. Generally, when the code length ≤ 64 , the proposed HMOH outperforms the second best, HCOH or BSODH by margins. In the case of 128-bit, HMOH yields a slightly better performance than its previous version, *i.e.*, HCOH. To explain, the Precision@K usually increases as the hash bit increases. Hence, HCOH can also obtain a relatively good performance in 128-bit. Nevertheless, the superiority of the proposed HMOH is consistent. Quantitatively, the proposed HMOH obtains an AUC improvement of 6.444%, 5.485%, 4.517%, 4.898%, 2.605% and 1.782% over the second best in 8-bit, 16-bit, 32-bit, 48-bit, 64-bit and 128-bit, respectively.

Lastly, we explore the impacts of different code lengths on the Precision-Recall performance on NUS-WIDE in Fig. 24. We conclude that on one hand, the proposed HMOH obtains the best performance overall, which verifies the effectiveness of the proposed HMOH on multi-label benchmark and the usefulness of the proposed “majority principle” and “balancedness principle”. On the other hand, similar to the mAP metric, the BSODH also shows the second

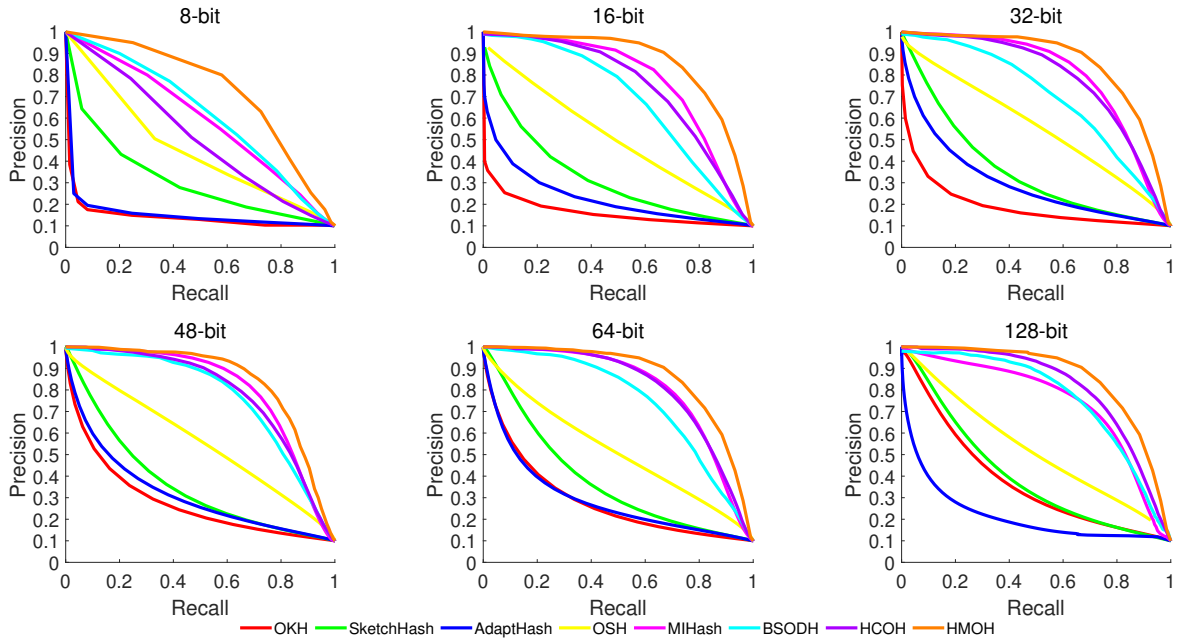


Fig. 19 Precision-Recall curves of compared algorithms on MNIST.

Table 5 mAP and Precision@H2 Comparisons on NUS-WIDE with 8, 16, 32, 48, 64 and 128 bits. The best result is labeled with boldface and the second best is with an underline.

Method	mAP						Precision@H2					
	8-bit	16-bit	32-bit	48-bit	64-bit	128-bit	8-bit	16-bit	32-bit	48-bit	64-bit	128-bit
OKH	0.337	0.341	0.350	0.345	0.348	0.352	0.336	0.340	0.381	0.319	0.183	0.004
SketchHash	0.368	0.373	0.375	0.377	0.375	0.379	0.381	0.430	0.375	0.082	0.027	0.002
AdaptHash	0.350	0.362	0.368	0.365	0.343	0.354	0.341	0.365	0.407	0.369	0.336	0.358
OSH	0.381	0.402	0.408	0.409	0.416	0.413	0.395	0.427	0.421	0.355	0.208	0.001
MIHash	0.360	0.343	0.347	0.349	0.348	0.354	0.370	0.372	0.365	0.361	0.355	0.345
BSODH	<u>0.430</u>	<u>0.437</u>	<u>0.440</u>	<u>0.438</u>	<u>0.438</u>	<u>0.440</u>	0.420	0.446	0.454	<u>0.455</u>	<u>0.457</u>	<u>0.459</u>
HCOH	0.398	<u>0.437</u>	0.430	0.431	0.432	0.428	0.400	<u>0.454</u>	<u>0.477</u>	0.409	0.346	0.153
HMOH	0.431	0.440	0.446	0.448	0.451	0.454	0.417	0.468	0.488	0.466	0.474	0.468

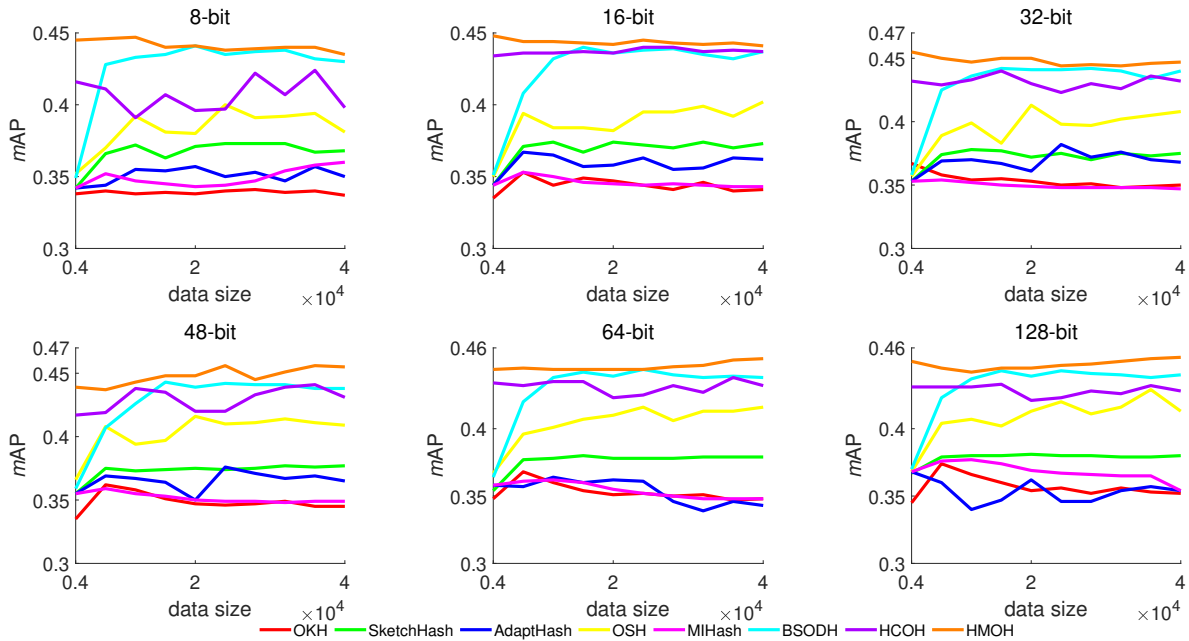


Fig. 20 mAP performance with respect to different sizes of training instances on NUS-WIDE.

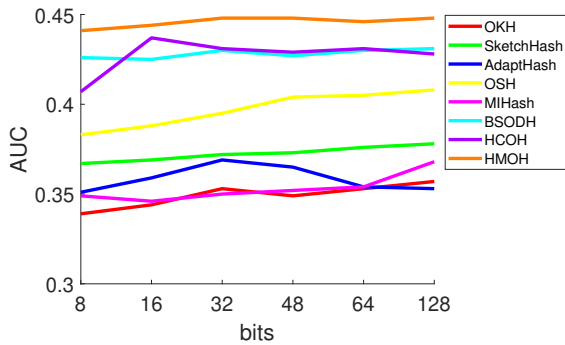


Fig. 21 AUC curves for mAP on NUS-WIDE.

best, which is even slightly better performance compared with the proposed HMOH in 48-bit due to the advantage of inner-product scheme in multi-label datasets.

To sum, the above four benchmarks give a strong verification of the effectiveness of the proposed method. It’s worth noting that in terms of Precision@K performance under 128-bit, the proposed HMOH ranks first, third, second and first on CIFAR-10 (Fig. 7), Places205 (Fig. 12), MNIST (Fig. 17) and NUS-WIDE (Fig. 23), respectively. However, regarding mAP ($mAP@1,000$), HMOH holds a consistently first position, which means that not only the proposed HMOH retrieves the relevant instances to the query sample, but also ranks them at the top of the list. It conforms with user experience in real-world applications. Besides, the classification based HMOH shows significant improvements over the regression based HCOH, which demonstrates that using a classification setting is a better choice comparing to using a regression setting. To explain, our method differs in the construction of Hadamard matrix, which serves as the target binary codes. Under such a setting, the binary codes are known in advance and can be regarded as discrete labels. And the hash functions aim to accurately predict the discrete label for each data. On the other hand, HCOH adopts the regression learning which estimates the mapping from the input variables to numerical or continuous output variables. Under such a setting, the gap between continuous space and discrete space makes it hard to fit well. Consequently, it has to quantize the variables in continuous space to discrete space, which inevitably brings more quantization error. Instead, we consider the classification learning in this paper, which attempts to estimate the mapping function from the input variables to discrete/categorical output variables, since the given binary label is discrete. Hence, HMOH shows superior performance than HCOH.

4.3 Retrieval on Unseen Classes

We further conduct experiments with unseen classes by following the experimental settings in (Sablayrolles et al., 2017) on all the four benchmarks. Similar to (Sablayrolles

et al., 2017), for each benchmark, 75% of the categories are treated as seen classes to form the training set. The remaining 25% categories are regarded as unseen classes, which are further divided into a retrieval set and a test set to evaluate the hashing model. For each query, we retrieve the nearest neighbors among the retrieval set and then compute the Precision@K. The experiments are done as the hashing bit set as 64. Fig. 25 shows the experimental results with respect to different methods. As can be seen from Fig. 25, the proposed HMOH shows consistently best performance on all four benchmarks, which demonstrates that HMOH can be well applied to scenarios with unseen classes compared with existing online hashing methods.

4.4 Performance in Longer Code Length

From Tab. 2, Tab. 3, Tab. 4 and Tab. 5, we can see that the mAP performance increases with the hash bit length. However, the performance seems still not saturated even when the code lengths are 128-bit. Following this, we further conduct experiments in the longer code length of 256-bit and 512-bit and show the experimental results in Fig. 26. As can be observed from Fig. 26, most methods achieve optimal performance in the case of 128-bit. As the code length continuously increases, the performance starts to decrease. To analyze, the longer code lengths (256-bit and 512-bit) brings more redundant information, which inevitably introduces damage to the retrieval performance. Hence, the 128-bit might be the optimal code length regarding the performance. Longer code lengths are not encouraged based on our experimental observations.

4.5 Ablation Study

In this section, we study the effects of the hyper-parameters including the bandwidth parameter η , the kernel size m , the learning rate λ , batch size n_t , and the usefulness of ensemble strategy. For convenience, all the experiments are conducted on the four benchmarks in term of mAP ($mAP@1,000$) under the code length of 32. The experimental results can be generalized to other code lengths as well.

Effect of Bandwidth Parameter η . In this experiment, we evaluate the performance of the proposed HMOH *w.r.t* different values of the bandwidth parameter η applied in the kernelization process. We report the experimental results in Fig. 27. It can be observed that plotted data shows convex curves for all benchmarks. Hence, it’s easy to decide the best η values. Quantitatively, when set as 8, 10, 6 and 10, we obtain the best mAP ($mAP@1,000$) of 0.645, 0.305, 0.847 and 0.438 for CIFAR-10, Places205, MNIST and NUS-WIDE, respectively.

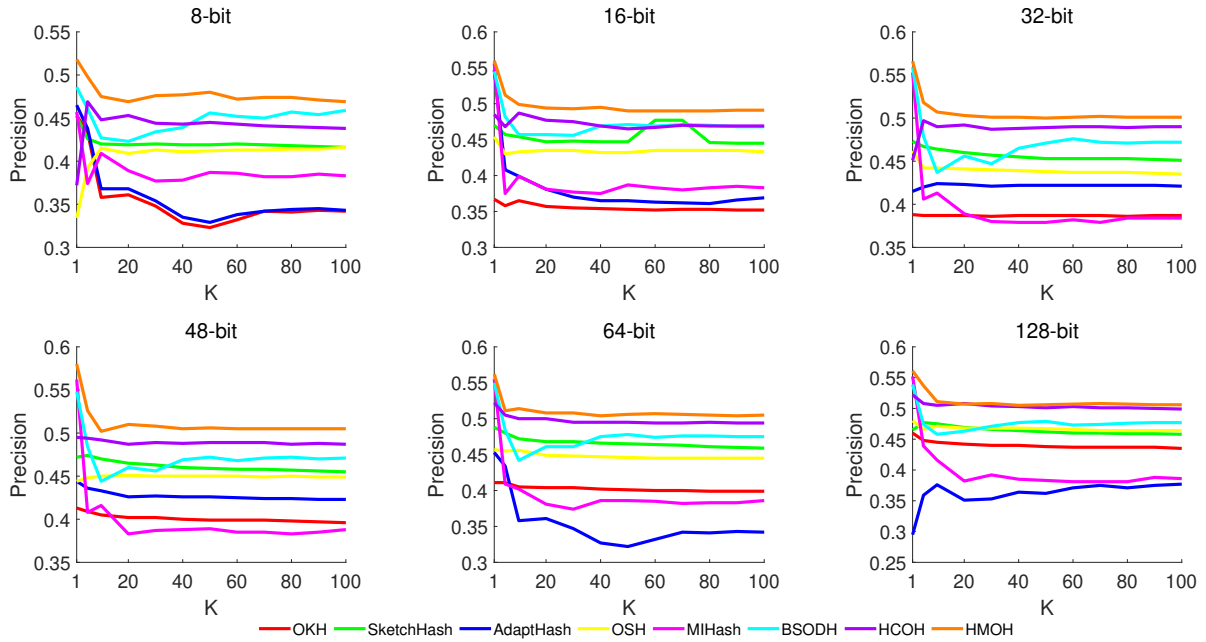


Fig. 22 Precision@K curves of compared algorithms on NUS-WIDE.

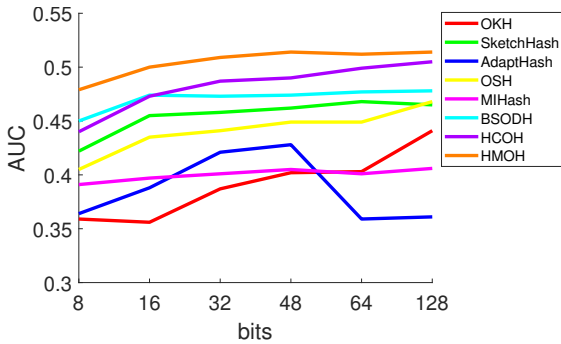


Fig. 23 AUC curves for Precision@K on NUS-WIDE.

Effect of Kernel Size m . In this part, we aim to evaluate the performance of the proposed HMOH regarding different sizes of kernel. The size of kernel not only affects the effectiveness but also the efficiency (Large kernel size brings more burdens on training time). Hence, the choice of kernel size m depends on the trade-off between effectiveness and efficiency. We plot these two factors in Fig. 28. Generally, as the kernel size increases, more training time is needed, while the performance of the proposed method first increases and then saturates. We can observe that the time curves for CIFAR-10 and MNIST overlap and the time cost for Places205 and NUS-WIDE are almost five times and two times as much as that of CIFAR-10 and MNIST. We analyze that this is because CIFAR-10 and MNIST have the same size of training instances (20K), while it is 100K for Places and 20K for NUS-WIDE. To take care of both effectiveness and efficiency, we choose m as 1000, 800, 300 and 500 for CIFAR-10, Places205, MNIST and NUS-WIDE, respectively.

During the experiments, we find that when applying the kernel trick on CIFAR-10 and NUS-WIDE, it doesn't do any benefit to the performance. Taking the hashing bit as 32 as an example, we obtain mAP of 0.645 and 0.446 without kernelization while it is only 0.305 and 0.438 with kernelization. We argue that this may be that CIFAR-10 and NUS-WIDE are linearly separable benchmarks in the original space. Therefore, for all the experiments related to CIFAR-10 and NUS-WIDE, we do not apply the kernel trick.

Effect of Learning Rate λ . The obtained mAP ($mAP@1,000$) with learning rate λ varying from 0.0001 to 1 are shown in Fig. 29. We can find that the proposed HMOH is not sensitive to λ in a large range, as HMOH achieves almost constant performance on all the four datasets. Nevertheless, in the experiments, we empirically set λ as 0.5, 0.01, 0.1 and 0.1 on CIFAR-10, Places205, MNIST and NUS-WIDE, respectively, with which we get mAP ($mAP@1,000$) of 0.723, 0.305, 0.847 and 0.446 on each dataset.

Effect of Batch Size n_t . This part of experiment mainly focuses on evaluating the effect of training size on the searching quality of the proposed HMOH. For simplicity, we choose the mAP as evaluation metric and vary the size of training data in the range of $\{1, 2, 3, \dots, 49, 50, 51, \dots, 100\}$. The experimental results are demonstrated in Fig. 30. As we can see, when the size increases from 1 to 100, we observe a slow decrease of the mAP performance. The precise values for $n_t = 1$ and $n_t = 2$ are 0.723 and 0.721, 0.305 and 0.290, 0.847 and 0.833, 0.446 and 0.441 on CIFAR-10, Places205, MNIST and NUS-WIDE, respectively. Such experimental results conform with the observations in HCOH (Lin

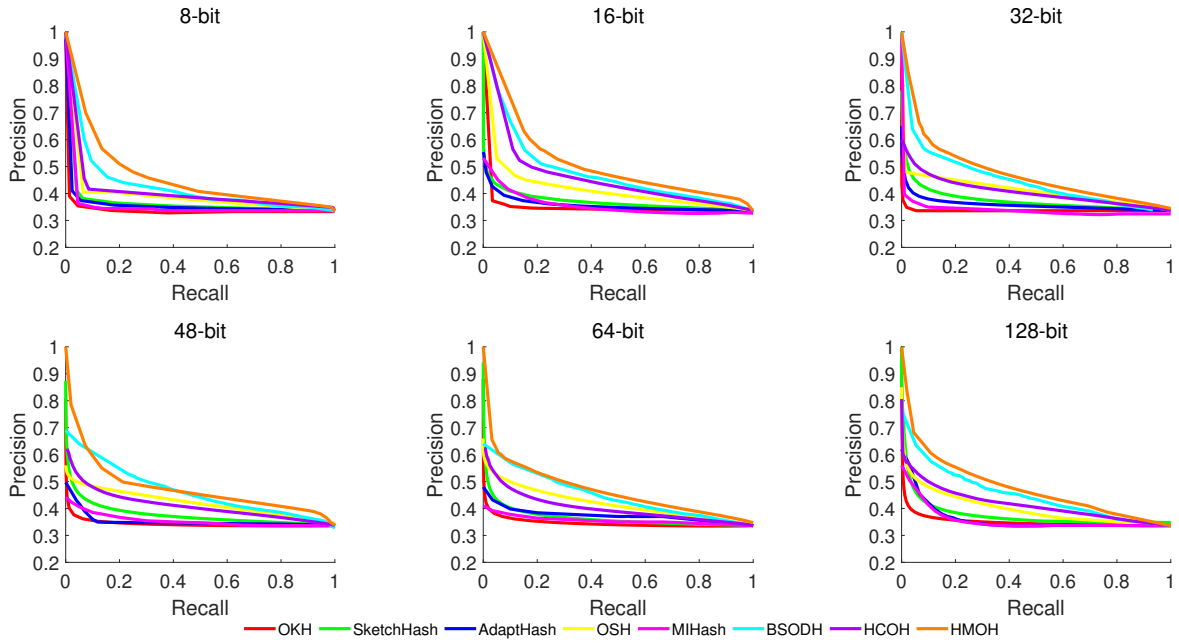


Fig. 24 Precision-Recall curves of compared algorithms on NUS-WIDE.

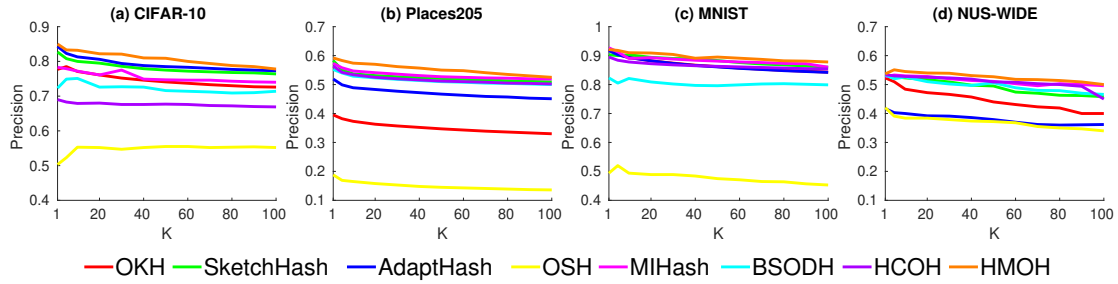


Fig. 25 Precision@K curves on unseen class when the hash bit is 64.

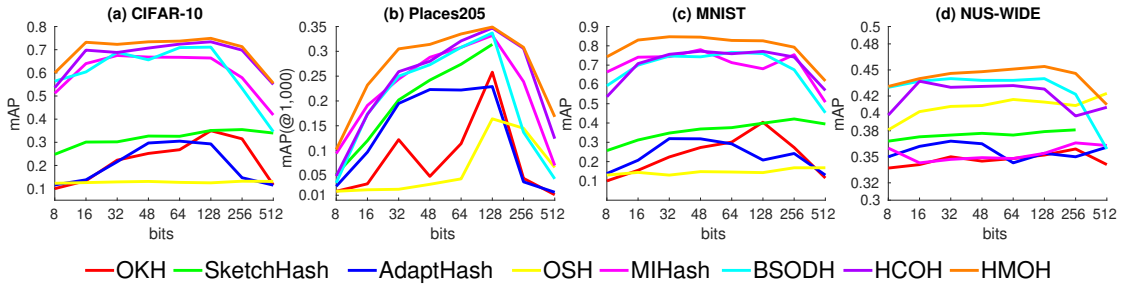


Fig. 26 mAP ($mAP@1,000$) curves with different code lengths.

et al., 2018). To explain, firstly, the Perceptron algorithm for classification adopted by nature updates the classifier instance-wise. Secondly, in online learning, the past stream data is not allowed to be reused to renew the models. To guarantee the learning efficiency, for each arriving stream data, the optimizer usually updates the model only once instead of iteratively. The number of training iterations significantly decreases as the batch size increases, which then degenerates the performance. Therefore, we leave the training size n_t set as 1 for all four datasets.

Effect of Ensemble Strategy. The quantitative evaluations for the effect of the ensemble strategy are shown in Fig. 31. The blue lines show the results with no ensembling while the red lines denote the results with ensembling. As can be observed, the ensemble strategy takes effect on all four benchmarks. Quantitatively, ensemble strategy obtains an average improvement of 14.439%, 23.365%, 6.716% and 15.245% on CIFAR-10, Places205, MNIST and NUS-WIDE, respectively. These experiments validate the

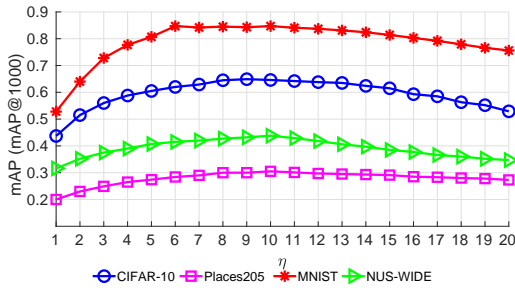


Fig. 27 mAP ($mAP@1,000$) with varying temperature parameters.

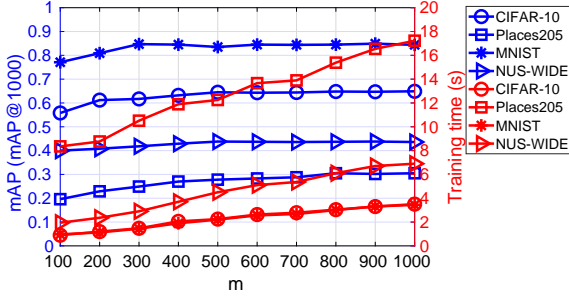


Fig. 28 mAP ($mAP@1,000$) over different sizes of kernel.

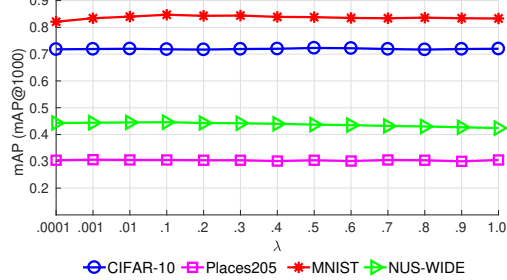


Fig. 29 mAP ($mAP@1,000$) with varying learning rates.

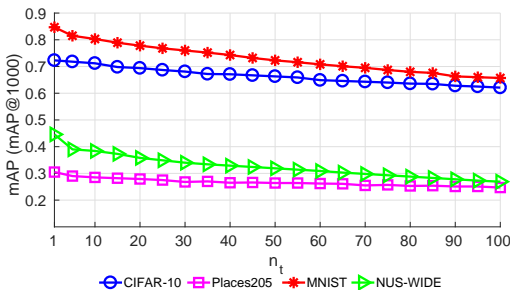


Fig. 30 mAP ($mAP@1,000$) over different sizes of batches.

importance of considering the past learnt information, which can boost the performance of online hashing.

4.6 Performance Variation on Places205

As stated in Sec. 4.1, in the Places205, 20 images from each categories are randomly sampled, consisting of a total of 4,100 query images. However, the large scale of Places205 (2.5 million) may introduce large performance variation due to the random selection. To test the performance variation,

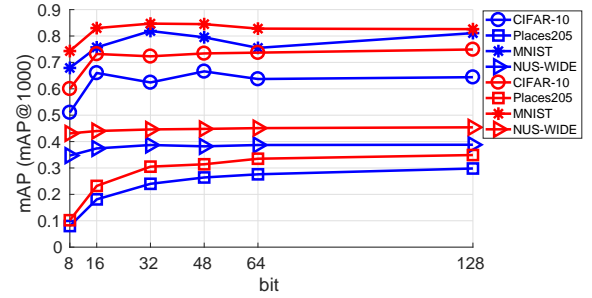


Fig. 31 Usefulness of the ensemble strategy (Blue lines denote the results without ensembling and red lines denote the results with ensembling).

we analyze the “mean \pm std” of $mAP@1,000$ in 32-bit. To that effect, the images sampled from each category range in $\{20, 30, 40, 50, 100, 200, 300, 400, 500\}$, composing of a test set of $\{4100, 6150, 8200, 10250, 20500, 41000, 61500, 82000, 102500\}$ images, respectively. The experimental results are shown in Tab. 6. As can be seen, the variations of most methods are small, and most methods are not sensitive to the size of test set, especially for state-of-the-art methods, *i.e.*, MIHash, BSODH, HCOH and the proposed HMOH. Besides, it can be observed that the proposed HMOH consistently show superiorities over the compared methods. Especially, in the case of 500 images sampled from each category which composes of a large testing set with 102,500 images, HMOH still yields the best result, and the performance is similar to the case of 20 images sampled from each category that composes of a testing set with 4,100 images. Hence, the proposed HMOH is robust to the large-scale benchmarks.

4.7 Training Efficiency

We quantitatively evaluate the efficiency of the proposed HMOH in Tab. 7 when hashing bit is set as 32. The reported training time is the summarization of all training batches. Generally speaking, SketchHash and OKH hold the best training efficiency, which however suffer poor effectiveness as analyzed before. To stress, regarding state-of-the-art methods, *i.e.*, MIHash and BSODH, both HMOH and HCOH are much more efficient. To make a comparison between HMOH (classification based hashing) and HCOH (regression based hashing), the former performs more efficiently on CIFAR-10, MNIST and NUS-WIDE. And, on Places205, HCOH is better. We notice that on Places205, the required kernel size m is 800 as in Tab. 1. However, the original feature dimension on Places205 is 128. The increased dimension needs more training time. For a fair comparison, we further test the training time of HMOH without kernelization. And it takes only 6.34 seconds for

Table 6 The performance variation analysis in the case of 32-bit on Places205.

Number	OKH	SketchHash	AdaptHash	OSH	MIHash	BSODH	HCOH	HMOH
20	0.122±0.008	0.202±0.002	0.195±0.003	0.022±0.002	0.244±0.004	0.250±0.002	0.259±0.001	0.305±0.003
30	0.102±0.015	0.213±0.001	0.200±0.000	0.023±0.001	0.245±0.002	0.246±0.001	0.256±0.002	0.297±0.002
40	0.105±0.006	0.214±0.001	0.193±0.006	0.023±0.001	0.246±0.003	0.244±0.002	0.254±0.002	0.297±0.002
50	0.106±0.009	0.213±0.003	0.198±0.001	0.022±0.001	0.246±0.001	0.245±0.001	0.255±0.003	0.298±0.002
100	0.098±0.008	0.212±0.001	0.193±0.003	0.023±0.001	0.245±0.003	0.247±0.003	0.256±0.001	0.300±0.002
200	0.110±0.004	0.213±0.001	0.193±0.005	0.023±0.001	0.247±0.001	0.247±0.001	0.253±0.001	0.301±0.003
300	0.097±0.011	0.211±0.001	0.193±0.001	0.023±0.002	0.247±0.002	0.248±0.003	0.257±0.002	0.301±0.001
400	0.098±0.017	0.211±0.001	0.193±0.002	0.024±0.001	0.246±0.004	0.247±0.002	0.256±0.002	0.299±0.002
500	0.097±0.015	0.211±0.002	0.193±0.001	0.023±0.002	0.244±0.001	0.246±0.001	0.256±0.001	0.300±0.001

Table 7 Training time (Seconds) on four benchmarks under 32-bit hashing codes.

Method	CIFAR-10	Places205	MNIST	NUS-WIDE
OKH	4.53	15.66	4.58	15.50
SketchHash	4.98	3.52	1.27	23.35
AdaptHash	20.73	14.49	6.26	15.94
OSH	93.45	56.68	24.07	65.24
MIHash	120.10	468.77	97.59	504.33
BSODH	36.12	69.73	4.83	33.32
HCOH	12.34	10.54	4.01	6.23
HMOH	9.29	28.57	2.76	5.21

HMOH compared with 10.54 seconds for HCOH. Hence, the classification based HMOH is significantly more efficient than regression based HCOH.

5 Conclusion

In this paper, we present an online hashing method which comes with the inspiration of Hadamard matrix. To this end, the streaming data from the same class is assigned with a unique column of the Hadamard matrix as its target code. And the hash functions aim to fit the assigned code. To that effect, the assigned code is regarded as virtual binary categories. The learning of hash functions is further transformed into learning a set of binary classification problem, which can be well solved by off-the-shelf kernelized perceptual algorithm. Moreover, To guarantee the consistency between length of target code and the number of hashing bit, LSH algorithm is applied and theoretical analysis is given. Lastly, we propose to ensemble the hashing models learned in every round by simply adding them to boost the performance. Extensive experiments demonstrate the effectiveness and efficiency of the proposed method.

Acknowledgements This work is supported by the National Key R&D Program (No. 2017YFC0113000, and No. 2016YFB1001503), Nature Science Foundation of China (No. U1705262, No. 61772443, No. 61572410, and No.61702136).

References

- Babenko B, Yang MH, Belongie S (2009) A family of online boosting algorithms. In: Proceedings of the ICCV (Workshops)
- Cakir F, Sclaroff S (2015) Adaptive hashing for fast similarity search. In: Proceedings of the ICCV
- Cakir F, Bargal SA, Sclaroff S (2017a) Online supervised hashing. CVIU
- Cakir F, He K, Bargal SA, Sclaroff S (2017b) Mihash: Online hashing with mutual information. In: Proceedings of the ICCV
- Chen X, King I, Lyu MR (2017) Frosh: Faster online sketching hashing. In: Proceedings of the UAI
- Chua TS, Tang J, Hong R, Li H, Luo Z, Zheng YT (2009) Nus-wide: A real-world web image database from national university of singapore. In: Proceedings of the ACM CIVR
- Cover TM, Thomas JA (2012) Elements of information theory. John Wiley & Sons
- Crammer K, Dekel O, Keshet J, Shalev-Shwartz S, Singer Y (2006) Online passive-aggressive algorithms. Journal of Machine Learning Research 7(Mar):551–585
- Datar M, Immorlica N, Indyk P, Mirrokni VS (2004) Locality-sensitive hashing scheme based on p-stable distributions. In: Proceedings of the ACM SoCG
- Deng C, Yang E, Liu T, Li J, Liu W, Tao D (2019a) Unsupervised semantic-preserving adversarial hashing for image search. IEEE TIP
- Deng C, Yang E, Liu T, Tao D (2019b) Two-stream deep hashing with class-specific centers for supervised image search. IEEE TNNLS
- Deng J, Dong W, Socher R, Li LJ, Li K, Fei-Fei L (2009) Imagenet: A large-scale hierarchical image database. In: Proceedings of the CVPR
- Freund Y, Schapire RE (1999) Large margin classification using the perceptron algorithm. ML
- Gionis A, Indyk P, Motwani R, et al. (1999) Similarity search in high dimensions via hashing. In: Proceedings of the VLDB
- Goh KS, Chang E, Cheng KT (2001) Svm binary classifier ensembles for image classification. In: Proceedings of the

- ACM CIKM
- Goldberg K (1966) Hadamard matrices of order cube plus one. *Proceedings of the AMS*
- Gong Y, Lazebnik S, Gordo A, Perronnin F (2013) Iterative quantization: A procrustean approach to learning binary codes for large-scale image retrieval. *IEEE TPAMI*
- Gui J, Liu T, Sun Z, Tao D, Tan T (2018) Fast supervised discrete hashing. *IEEE TPAMI*
- Horadam KJ (2012) Hadamard matrices and their applications. Princeton university press
- Huang LK, Yang Q, Zheng WS (2013) Online hashing. In: *Proceedings of the IJCAI*, pp 1422–1428
- Huang LK, Yang Q, Zheng WS (2017) Online hashing. *IEEE TNNLS*
- Jiang J, Tu Z (2009) Efficient scale space auto-context for image segmentation and labeling. In: *Proceedings of the CVPR*
- Kittler J, Ghaderi R, Windeatt T, Matas J (2001) Face verification using error correcting output codes. In: *Proceedings of the CVPR*
- Krizhevsky A, Hinton G (2009) Learning multiple layers of features from tiny images. Technical report, University of Toronto
- Krizhevsky A, Sutskever I, Hinton GE (2012) Imagenet classification with deep convolutional neural networks. In: *Proceedings of the NIPS*
- Kulis B, Grauman K (2012) Kernelized locality-sensitive hashing. *IEEE TPAMI*
- LeCun Y, Bottou L, Bengio Y, Haffner P (1998) Gradient-based learning applied to document recognition. *Proceedings of the IEEE*
- Leng C, Wu J, Cheng J, Bai X, Lu H (2015) Online sketching hashing. In: *Proceedings of the CVPR*
- Liberty E (2013) Simple and deterministic matrix sketching. In: *Proceedings of the ACM SIGKDD*
- Lin M, Ji R, Liu H, Wu Y (2018) Supervised online hashing via hadamard codebook learning. In: *Proceedings of the ACM MM*
- Lin M, Ji R, Liu H, Sun X, Wu Y, Wu Y (2019) Towards optimal discrete online hashing with balanced similarity. In: *Proceedings of the AAAI*
- Liu D, Zhang P, Zheng Q (2015) An efficient online active learning algorithm for binary classification. *PRL*
- Liu H, Lin M, Zhang S, Wu Y, Huang F, Ji R (2018) Dense auto-encoder hashing for robust cross-modality retrieval. In: *Proceedings of the ACM MM*
- Liu W, Wang J, Ji R, Jiang YG, Chang SF (2012) Supervised hashing with kernels. In: *Proceedings of the CVPR*
- Liu W, Mu C, Kumar S, Chang SF (2014) Discrete graph hashing. In: *Proceedings of the CVPR*
- Lu Y, Dhillon P, Foster DP, Ungar L (2013) Faster ridge regression via the subsampled randomized hadamard transform. In: *Proceedings of the NIPS*
- Norouzi M, Blei DM (2011) Minimal loss hashing for compact binary codes. In: *Proceedings of the ICML*
- Novikoff AB (1963) On convergence proofs for perceptrons. Tech. rep., STANFORD RESEARCH INST MENLO PARK CA
- Ockwig NW, Delgado-Friedrichs O, O’Keeffe M, Yaghi OM (2005) Reticular chemistry: occurrence and taxonomy of nets and grammar for the design of frameworks. *Accounts of chemical research*
- Paley RE (1933) On orthogonal matrices. *Studies in Applied Mathematics*
- Peterson WW, Weldon EJ (1972) Error-correcting codes. MIT press
- Sablayrolles A, Douze M, Usunier N, Jégou H (2017) How should we evaluate supervised hashing? In: *Proceedings of the ICASSP*
- Schapire RE (1997) Using output codes to boost multiclass learning problems. In: *Proceedings of the ICML*
- Shen F, Shen C, Liu W, Tao Shen H (2015) Supervised discrete hashing. In: *Proceedings of the CVPR*
- Simonyan K, Zisserman A (2014) Very deep convolutional networks for large-scale image recognition. *arXiv preprint arXiv:14091556*
- Sylvester JJ (1867) Lx. thoughts on inverse orthogonal matrices, simultaneous signsuccessions, and tessellated pavements in two or more colours, with applications to newton’s rule, ornamental tile-work, and the theory of numbers. *The London, Edinburgh, and Dublin Philosophical Magazine and Journal of Science*
- Wang J, Kumar S, Chang SF (2010) Semi-supervised hashing for scalable image retrieval. In: *Proceedings of the CVPR*
- Wang J, Zhang T, Sebe N, Shen HT, et al. (2018) A survey on learning to hash. *IEEE PAMI*
- Weiss Y, Torralba A, Fergus R (2009) Spectral hashing. In: *Proceedings of the NIPS*
- Williamson J, et al. (1944) Hadamard’s determinant theorem and the sum of four squares. *Duke Mathematical Journal*
- Yang E, Deng C, Li C, Liu W, Li J, Tao D (2018) Shared predictive cross-modal deep quantization. *IEEE TNNLS*
- Zhao B, Xing EP (2013) Sparse output coding for large-scale visual recognition. In: *Proceedings of the CVPR*
- Zhou B, Lapedriza A, Xiao J, Torralba A, Oliva A (2014a) Learning deep features for scene recognition using places database. In: *Proceedings of the NIPS*
- Zhou J, Ding G, Guo Y (2014b) Latent semantic sparse hashing for cross-modal similarity search. In: *Proceedings of the ACM SIGIR*